Master's Thesis – Master in Energy Science

Location optimization of wind and solar power plants in Northwest Europe

Teun Strikkers, BSc.

t.strikkers@students.uu.nl
6218989

16/08/2019

Supervisors

Prof. Dr. Madeleine Gibescu

Jing Hu, MSc.

Utrecht University

Cover Image: [1]

Abstract

In light of climate change mitigation, the European Union and its member states aim to increase their share of renewable energy in the energy system. Some of these resources, such as wind turbines and solar PV panels produce Variable Renewable Electricity (VRE). Due to its intermittent nature VRE can pose a problem to this system. Numerous research has looked into addressing the variability by strategically placing VRE technologies in a large geographical area so that their variance is decreased or their correlation with the electricity demand is increased. This thesis uses portfolio theory to further investigate how VRE technologies can better be integrated in the electricity system by maximizing the covariance between VRE production and electricity demand. Northwest Europe is chosen as a case study area and the temporal scope was set at 2030. In addition, Demand Response (DR) is added to the optimization to further investigate maximizing this covariance. An unconstrained, constrained and constrained DR scenario are created. The results show that the unconstrained scenario exhibit the highest covariance across all scenarios and the maximum covariance portfolio of this scenario has an increase of 55 % compared to the maximum return portfolio. However, the variance of the unconstrained scenarios is also higher. The correlation coefficient between VRE production and demand is also calculated. By using DR, a maximum correlation of 0.29 is attained. This demonstrates that while the unconstrained covariance analysis yields the highest return and covariance, the constrained scenarios exhibits lower variance and higher correlation. The results indicate that maximizing the covariance might not be the best optimization technique to determine the most optimal integration of VRE technologies in the energy system as maximizing correlation or minimizing variance is potentially better. Nevertheless, DR contributes to both maximizing the covariance and correlation. Furthermore, the results show that attention should be given to what extend and where VRE assets should be installed from an energy system point of view, because they can alter the variance of production, production itself, as well as the covariance and correlation between production and demand.

Preface

In front of you lies the culmination of 5 years of academic studies. During this time, climate change has shifted from being something that mostly occurs in the future to something that occurs at this very moment. The Paris agreement was signed during this time, indicating that society wants to curb the effects of climate change. Part of the solution is changing the way society uses and produces energy. The change of such a complex system requires vast alterations and new technologies. This thesis aims at increasing the understanding of one of these solutions, strategically placing of VRE assets so that they are able to better integrate in the energy system. This is important as potentially it can reduce the need of other resources and technologies while increasing energy security.

Table of Contents

List of Figures

List of Tables

Abbreviations

CF	Capacity Factor
CLC	Corine Land Cover
DR	Demand Response
DHI	Diffuse Horizontal Irradiance
DNI	Direct Normal Irradiance
ECMWF	European Centre for Medium-Range Weather Forecasts
EU	European Union
GHI	Global Horizontal Irradiance
IEC	International Electrotechnical Commission
MCVA	Mean Covariance Analysis
MVA	Mean Variance Analysis
NaN	Not a Number
PV	Photovoltaic
SAPM	Sandia PV Array Performance Model
SD	Standard Deviation
SSRD	Surface Solar Radiation Downwards
VRE	Variable Renewable Energy

Nomenclature

a	Asset
θ	Angle of incidence
β	Tilt
θ_z	Solar zenith angle
γ	Relative azimuth
I_{POA}	Total irradiance on a tilted plane of array
$I_{POA_{direct}}$	Direct irradiance received on a plane of array
$I_{POA_{dif,sky}}$	Sky diffuse irradiance received on a plane of array
$I_{POA_{dif,reflect}}$	Sky reflect irradiance received on a plane of array
σ_a	Albedo
α_i	Anisotropy index
DNI_{extra}	Extra-terrestrial irradiance
$P_{eff,a,t}$	Effective power output of asset a at time t
P_{dc0}	Rated power of solar cell
$\gamma_{pdc,x}$	Temperature coefficient of module
$T_{cell,a,t}$	Cell temperature of asset of asset a at time t
T_{ref}	Reference temperature (25 °C)
PR	Performance Ratio
u_{10m}	Wind speed at 10 meters
$T_{i,t}$	Outdoor temperature at 2 meters
CF	Capacity Factor
u	Wind speed
h	Height
z_0	Surface Roughness
σ_n	Normalised standard deviation
σ_w	Wind speed standard deviation according to [2]
k	Wind speed offset
Ps	Discrete single turbine power curve element

ps	Probability Distribution
Pm	Adjusted turbine power curve element
η_{wake}	Wake efficiency
η_{avail}	Availability of Turbines
f_i	Suitability Factor
a_i	Area weighting
ω_i	Land cover suitability
b_i	Nature reserve suitability
A_{panel}	Area solar PV panel
A_{used_tilted}	Used titled area
A_{used}	Used area
α_{ref}	Reference solar altitude
$\hat{p}$	Maximum power density
D	Diameter
c^{max}	Maximum power constraint
$E_{t,2030,country}$	Adjusted to 2030 electricity demand for $country$
$E_{t,2030}$	Electricity demand in 2030
d_e	Electricity demand
$\alpha_{year,country}$	Expected increase in demand from $year$ to 2030
$E_{2030,country}$	Expected electricity demand country
r_p	Return portfolio
w_a	Weight of asset a
d	Normalized electricity demand
ca_{VRE}	Expected installed VRE capacity
ca_a	Expected installed VRE capacity per technology for each country
$\rho_{d,p}$	Correlation between electricity demand the return of the portfolio
σ_p	Standard deviation portfolio
σ_d	Standard deviation demand

1. Introduction

Considering climate change mitigation, the uptake of renewable energy technologies in the European Union (EU) will further increase in the future [3]. Herein solar Photovoltaic (PV) and wind power play an important role. The 2030 EU energy framework target states that 32% of the final energy consumption must come from renewable resources by 2030 [4]. It has been shown that in the case of Germany if the share of solar PV and wind turbine exceeds 30% of the total energy production that either energy has to be wasted, transported or stored [5]. The growth of VRE can therefore be a problem for the electricity system as especially these two resources are weather dependent and produce Variable Renewable Electricity (VRE) [6]. The electricity system traditionally relies on power production that is manageable in terms of when production can be turned on or off. VRE being variable makes it thus more difficult to balance supply and demand. Especially when injecting larger shares of wind and solar energy in the system than that are currently installed [5,7,8].

Several technologies and methods have been proposed to accommodate the variability of VRE [6,9]. They aim to solve this variability by either controlling power production, energy storage, increasing interconnection or Demand Response (DR) [5,10]. DR means demand pattern can be altered by using e.g. smart grids, or altering the time of industrial energy intensive production [5,11].

However, there is also another option that is not able to accommodate the variability at the source of the problem, before it arises. This solution is to strategically place wind turbines and solar panels at different locations in a larger area [12,13]. This placing has the aim to put the VRE technologies in places where in total they can produce electricity with the smallest possible variation in production or follow the demand most closely. Especially combining wind and solar can increase VRE stability in the electricity grid [13,14]. The amount of additional options needed to integrate the shares of VRE can therefore be decreased. However, the premise of most of the strategic installation VRE research is the 'copper plate' assumption [13–16], meaning that electricity can be transported freely inter and intra country. This means that if VRE technologies are strategically placed additional funding could still be necessary for increasing the transmission grid.

1.1 Literature Review

Multiple methods have been used to identify sets of optimal locations of VRE technologies to reduce energy production variability [13,17–19]. An overview of their research is summarized in Table 1-1. It shows that there is a high variation in the way research is conducted, in their inclusion of VRE technologies as well as in data sources and spatial resolution. Generally, these studies use multi-year weather or electricity data. The optimization in these studies was performed to reduce the residual between energy demand and production using nonlinear optimization [19] or linear least square regression [16,18]. Other studies aimed at maximizing power production/capacity factor while minimizing the volatility in (hourly) production using portfolio theory [13,15,20], or minimizing the variability of wind power and the ratio of energy variability and energy input [17]. While the characteristics differ, these studies showed that a reduction in VRE variability leads to overall lower maximum power production compared to maximizing for power production.

However, some of this research does not explicitly consider electricity demand [13,15,20]. Including electricity demand in the optimization will improve the optimization as electricity production variation that matches the electricity demand is not penalised. Other studies do include electricity demand [16,18,19], however, these studies only use a few year(s) of electricity demand data while using 40 years of weather data. The disadvantage of this is that the link between weather patterns, e.g. rise in solar irradiance and temperature, do not correspond well to the electricity demand at that time. Furthermore, these studies either optimized for maximum power production or minimal residual demand. This means that trade-offs between having maximum power production or exactly following demand could be overlooked. For example, when minimizing solely for variability it is unclear how much variability needs to be "sacrificed" to gain more renewable electricity output. This demonstrates the advantage of using portfolio theory, as it not only shows the solution at maximum return or minimum production but also identifies the solution in between these points which can show these trade-offs [12,13,15,21,22].

Table 1-1: Summary of selected previous research on reducing the variability of VRE in the electricity system.

Authors	Optimization	Wind turbines	Solar PV	Spatial resolution	Locations included	Electricity demand matched in optimization	Demand Response	Ranged solutions[3.]
Cassola, Burlando, Antonelli, & Ratto [10]	Minimizing wind power variability	✓	×	Individual weather station data	×	×	×	×
Grossmann, Grossmann, & Steininger [18]	Selecting out of 67 pre-defined sites to reduce solar PV variability	×	✓	1° (~110 x 90 km)	✓ [1.]	✓	× [2.]	×
Van der Vliet [19]	Matching the VRE production with the electricity demand	✓	✓	0.5°	✓	✓	× [2.]	×
Zappa & Van den Broek [16]	Mixing the spatial distribution of VRE to minimise residual load by maximizing the correlation.	✓	✓	0.75°	✓	✓	×	×
Portfolio theory based research								
Rombauts, Delarue, & D'haeseleer [14]	Maximizing the average capacity factor of wind power while minimizing hourly wind power fluctuations	✓	×	Individual weather station data	×	×	×	✓

Roques, Hiroux, & Saguan [13]	Maximizing wind power production and minimizing variability, at all times and specifically during peak hours	✓	×	National wind power production	×	×	×	✓
Shahriari & Blumsack [9]	Aggregation of wind and solar PV power plants to increase the overall availability factor.	✓	✓	2 km x 2 km	✓ [1.]	×	×	✓
Hu, Harmsen, Crijns-Graus & Worrell [14]	Reducing the variance of wind and solar PV assets while maximizing their return	✓	✓	0.5° x 0.667°	✓	×	×	✓
Tejeda, Gallardo, Domínguez, et al. [23]	Reducing the variability of wind output	✓	✓	0.25° x 0.25°	✓	✓ [4.]	×	✓

[1.] Given in aggregated large regions. [2.] Storage is used for curtailment. [3.]Ranged solutions refers to finding sets of locations that show solutions not only at the extremes, e.g. where the variability is minimized or the output is maximized, but also the solutions that lay in between these points. [4.]Unclear if hourly demand pattern is used. Uses one year of demand data.

Portfolio theory is an economic theory first coined by Markowitz in 1952 [24]. A portfolio refers to collection of assets [25]. Each distinct portfolio has a unique division of the shares of the assets. Originally this theory aimed to select optimal portfolios consisting of sets of investments that reduce the risk compared to selecting just an individual investment. Diversifying the assets in the portfolio the right way can reduce the risk and increase the return. The theory stipulates that the set of optimal portfolios should have a maximum return for each level of risk. This set of portfolios constitute the efficient frontier, an example is shown in Figure 1. Every point on the line represents a portfolio that cannot increase its return without increasing its risk or decreasing its risk without reducing its return [15]. The return, originally refers to the expected return of an investment, and risk, to the variance of return of the portfolio. In short, the theory outlines that picking the "right" set of investments decreases the variance compared to picking one investment.

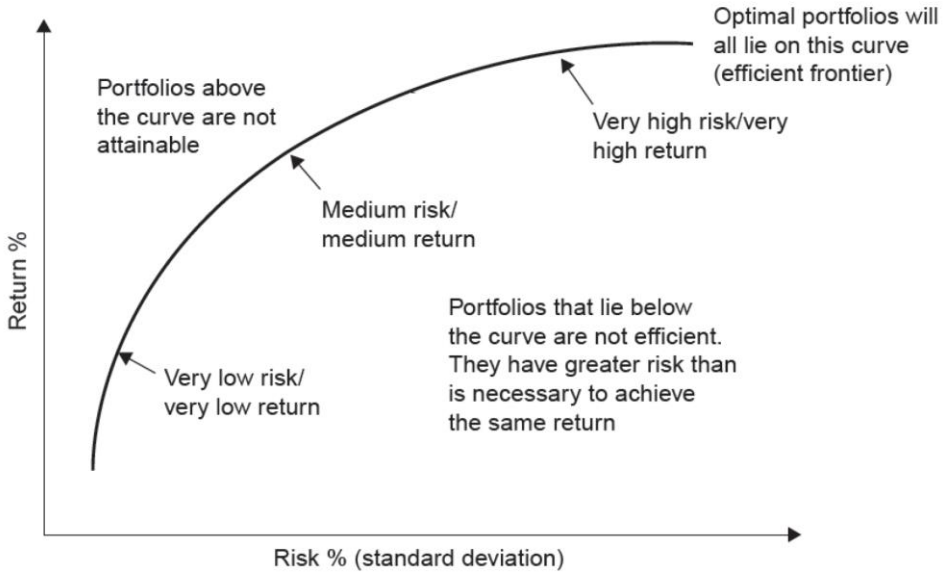

Figure 1: Efficient frontier risk refers to the variability [12]

When applying portfolio theory to energy system planning, the expected return can either be the investment cost of the new technologies in the energy system, the actual financial return or the energy produced [21]. The variability can refer to the variability in cost, in financial return or in energy produced. Generally, the asset is replaced by locations of VRE or different energy sources. Applying portfolio theory to energy planning is favourable compared to other methods because it can produce portfolios of wind and solar technologies that minimize the variability of VRE, while

also showing the trade-offs between having high return (energy output) or low variability (VRE variability) [13].

The results of portfolio analysis can be a set of portfolios consisting of VRE technologies that have maximized electricity produced under the same variability, or portfolios that have minimized variability under the same electricity produced [20]. These portfolios construct the efficient frontier from the point where the variance is globally minimized to the point where the return is globally maximized [15]. Therefore, using portfolio theory makes it possible for policy makers or system operators to identify optimal locations of VRE power plants. They can opt to optimize locations to either having more renewable energy produced or having less volatile energy production, allowing for more insightful decision making. Also, if policy makers or system operators know what level of production variability the system can accommodate, they can identify what maximum energy output can be achieved, subject to their maximum variability constraint. They could promote these regions so that energy producers or prosumers are more inclined to install VRE technologies in these regions.

Previous portfolio-based research, however, did not look at matching the VRE production and demand since they analysed the variance of production or the monetary variance [13,15,20,21]. Matching the electricity demand profile more closely with VRE generation will identify locations of these power plants that can be more easily accommodated in the electricity system. To better match the supply and demand, the covariance between energy demand and VRE production could be used instead of the variance itself. Doing so would identify portfolios that have various degrees of covariance, meaning that they either perform better or worse in relation to matching the energy demand, while exploring the trade-off with higher or lower energy production. Including covariance thus extends the application of portfolio theory in energy systems planning.

To further investigate the potential of maximizing the covariance between VRE and electricity demand, Demand Response (DR) was investigated. DR or demand side management refers to activities that alter the demand profile of electricity consumer both in time and in level to balance the electricity system [26–28]. This can entail to lower or shift the consumers' demand during peak load time [29] or to balance intermittent (VRE) generation [28,30]. Until now, literature has identified that there is a considerable potential for DR in the European power market and that the

implementation can change the optimal mix of wind and solar [27,31]. It is therefore beneficial to investigate the role of DR on the relationship between VRE production and demand and how this affects the overall division of wind and solar.

As a case study area, Northwest Europe is chosen. The relatively small size allows for reasonable computation time to solve the optimization while also maintaining enough weather variability to find different solutions [19]. The temporal scope is set at 2030 so that changes in weather patterns and land use were minimal.

1.2 Research Questions

Based on the literature mentioned above, this thesis aims to answer the following research questions:

- To what extent can the covariance between VRE production and demand be maximized for each attainable energy output level, in Northwest Europe?
- What are the optimal spatial distributions for wind and solar assets in Northwest Europe, that maximize the covariance and return?
- To what extend can DR maximize the covariance between VRE production and energy demand?

The covariance analysis builds on mean variance portfolio analysis. The result of this analysis is the expected return, being the VRE produced, and the covariance between energy demand and energy produced. The result of this optimization determines both the extend, where the trade-off between covariance and return are and the locations of the VRE technologies. The third question helps to further investigate the covariance between VRE production and demand as part of the demand pattern can be altered.

The outline of this thesis is as follows. Chapter 2 describes the methodology. Chapter 3 shows the results of both the key intermediate steps as well as the results of the portfolio analysis. The results are discussed in chapter 4, discussion. Chapter 5, describes the conclusion.

2. Data & Methodology

This chapter adumbrates the steps taken to attain answers to the research questions. Its foundation is based on a multitude of studies [13–16,20,32]. Figure 2 shows the overall main methodological steps of this thesis. For the optimization, *Python*, *R Studio, ArcMap* and *Excel* were used, at each subsection the respective programme is mentioned as well as in Figure 2. Before data gathering started, the geographic area was defined. Belgium, Denmark, Germany, Ireland, Luxembourg, the Netherlands, Norway and the United Kingdom were set as the countries belonging to Northwest Europe. In Arcmap various maps were combined to get the country outlines and sea borders [33–35]. This thesis used the Exclusive Economic Zones to define borders at sea [31] and set a limit was imposed at 100 km from shore for wind offshore, in line with [15,32].

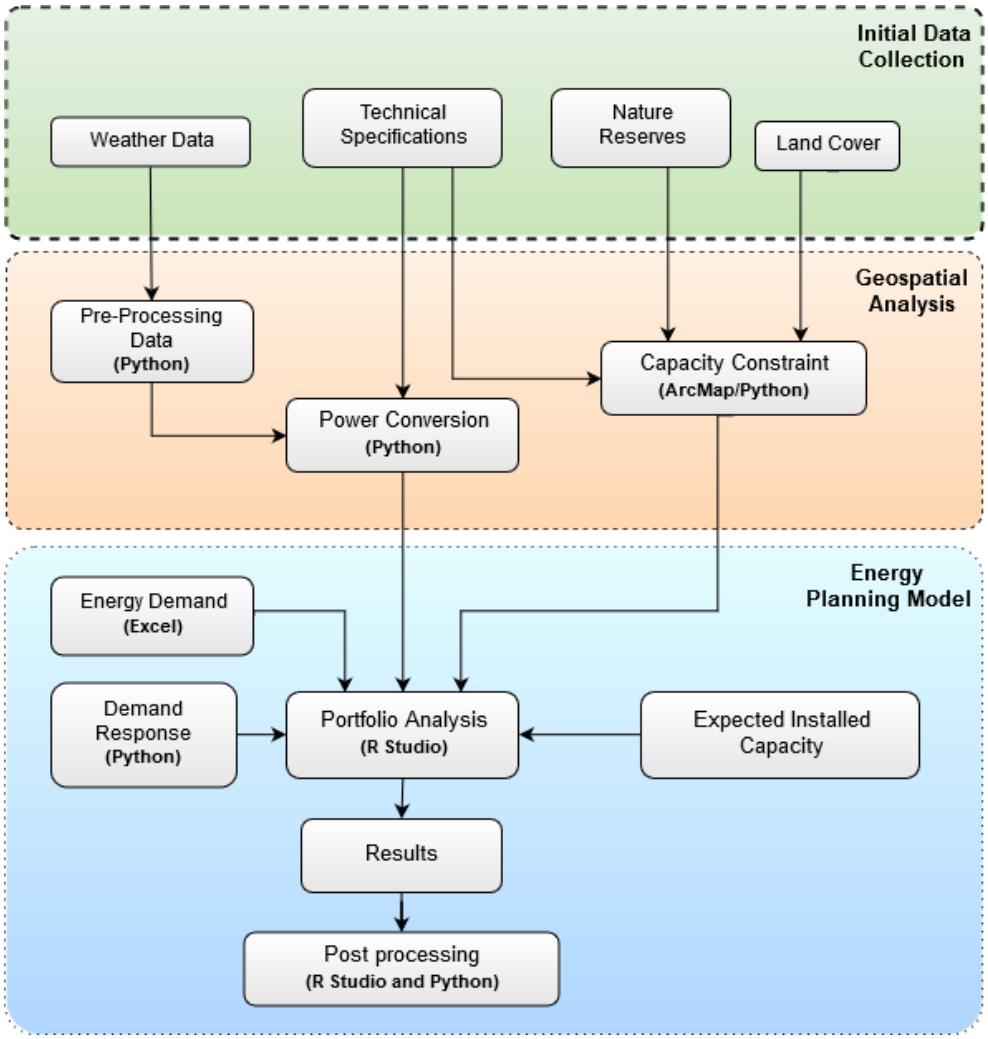

Figure 2: Flow chart of designed energy model

The outline of this chapter mirrors the outline diagram. Section 2.1 addresses the weather data. The pre-processed weather data is thereafter combined with the technical specifications of wind turbines and solar PV panels to produce the hourly power output, defined in section 2.2 Power Conversion. In that section the power output is first calculated in power/hour, after which it is converted to hourly capacity factor. Next, additional technical data is used together with geographical information on land cover and bio reserves to determine the capacity constraint in section 2.3. The expected installed capacity in 2030 and the energy demand are discussed respectively in section 2.4 & 2.5. The energy demand, expected installed VRE capacity, hourly power output and the capacity constraints all serve as input for the portfolio analysis, see section 2.6. The demand response optimization is outlined in section 2.7 and the post processing of the results is described in section 2.8. The results of the portfolio analysis are presented in chapter 3.

2.1 Weather Data

The hourly electricity production by VRE technologies was determined using the hourly weather data for Northwest Europe at uniform spatial resolution. Numerous datasets are available to compute this [36,37]. ERA5, is a recent reanalysis weather dataset developed by the European Centre for Medium-Range Weather Forecasts (ECMWF) and uses past measurements and models to map out the weather [38,39]. Contrary to its predecessor, ERA-Interim, ERA5 has higher geographic resolution data (0.25° x 0.25°, versus 0.7° x 0.7°) and hourly intervals as well as wind speed at 100 m [38]. Even though this resolution is low compared to satellite data [36], the weather variation between two grid cells of 0.25° low [16], meaning that an increase in resolution will not affect the results in a considerable way. Furthermore, ERA5 is shown to be more accurate than another widely used weather dataset, MERRA-2, for both wind and solar power production [36,37]. Therefore, coupled with a reduction in computation time compared to satellite data, this study used the ERA5 dataset for the input weather data.

The ERA5 data is pre-processed such that it is trimmed exactly to the right dimension of the case study area. The variables used for this study and for what technology can be seen in Table 2-1. They are further explained in their respective sections. VRE technologies, x, that are installed in locations i are referred to as assets, a.

Table 2-1: ERA5 variables used in this thesis.

Variable in ERA5	Translated meaning	Section
SSRD	Global Horizontal Irradiance	2.2.1 Solar power conversion
FDIF	Diffuse Horizontal Irradiance	2.2.1 Solar power conversion
FDIR	Direct Normal Irradiance	2.2.1 Solar power conversion
T2m	Temperature at 2m	2.2.1.VII PV array Model
Wspdrf	Wind speed at 10m	2.2.1.VII PV array Model
Wspd100	Wind speed at 100m	2.2.2 Wind Power Conversion

2.2 Power Conversion

The following section explains the steps taken to convert the hourly weather data into hourly capacity factor. First, the conversion of irradiance data into solar power is addressed. Second, the power conversion of wind speed in wind power is described.

2.2.1 Solar PV Power Conversion

Several methods exist to convert incoming solar irradiance into power output [40–43]. Some of the models do not take into account the diffuse component solar irradiance due to its reduced computation time [40,41], thereby accepting a loss of at least 10% in the power output [43]. However, this study took the diffuse component into account as it more accurately represents reality. This thesis follows the model as depicted in Figure 3 to calculate the solar PV power output. To do this the PVLib Python library [42] was used for the computation of solar power due to its extensive modelling possibilities[44]. The next subsections address each of the model points, starting with the solar irradiance.

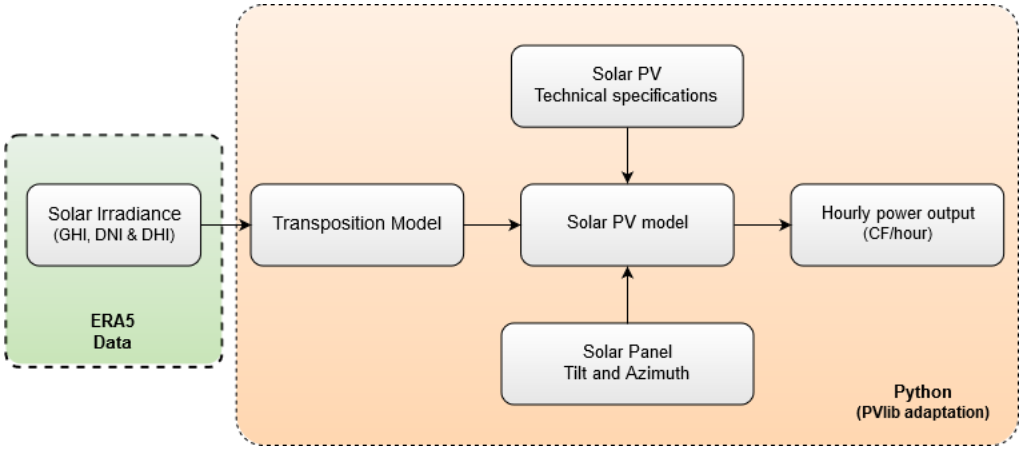

Figure 3: Model outline Solar PV power conversion based on [42,45,46]

I. Irradiance

The irradiance data was taken from the ERA5 dataset [38]. On a horizontal surface, the solar radiation or Global Horizontal Irradiance (GHI), is given by *(1)*.

$$GHI = DNI + DHI \tag{1}$$

Where DNI is the Direct Normal Irradiance (DNI), and DHI is the Diffuse Horizontal Irradiance which represents the diffuse component [43]. The ERA5 dataset gives the Surface Solar Radiation Downwards (SSRD) in J/m^2 as GHI which has to be converted to W/m^2 [16,47] using *(2)*.

$$P = \frac{E}{t} \tag{2}$$

Where P is the power per m^2, E is the energy per m^2 and t the time in seconds in each time step. To compute the irradiance on a tilted surface the direct solar beam (DNI) and the diffuse radiation are also needed (DHI) [43]. In ERA5 notation [48], DNI is referred to as FDIR. DHI is not given by ERA5 and is calculated by *(3)*.

$$DHI = GHI - DNI \tag{3}$$

Consequently, both the DHI and DNI are converted using *(2)* to get their outputs in W/m^2.

II. Transposition models

Once the diffuse beam is known, GHI, DHI and DNI were used in a transposition model to determine the irradiance received on the Plane Of Array (POA), or tilted surface [43,49]. Generally, there are two types of transposition models that determine the sky diffuse radiation on a tilted solar panel, isotropic and anisotropic [50,51]. Isotropic models include three radiation components to determine the radiation, direct beam, isotropic diffuse and reflected solar radiation [51]. Anisotropic build on the isotropic model and also includes circumsolar diffuse as well as diffuse form horizon radiation [51]. Numerous studies have evaluated the accurateness of the different transposition models [50–57]. However, these studies do not overlap in what models are selected for their study, making comparison difficult.

This study used the Reindl transposition anisotropic model [45,58,59]. The POA irradiance, according to the Reindl model can be calculated using equation *(4)*, which the Python library has an integrated tool for.

$$I_{POA} = I_{POA_{direct}} + I_{POA_{dif,sky}} + I_{POA_{dif,reflect}} \quad (4)$$

Where $I_{POA_{direct}}$ is the direct irradiance received on the plane, $I_{POA_{dif,sky}}$, the diffuse radiation from the sky, and $I_{POA_{dif,reflect}}$, the diffuse radiation reflected from the ground. $I_{POA_{direct}}$ is calculated using *(5)*.

$$I_{POA_{direct}} = DNI \cos\theta \quad (5)$$

Where θ is the angle of incidence. It was calculated using the solar zenith angle θ_z, the relative azimuth,γ, and the tilt of the panel, β, see *(6)*

$$\cos\theta = \cos\beta \cos\theta_z + \sin\beta \sin\theta_z \cos\gamma \quad (6)$$

The ground reflected diffuse irradiance is given by *(7)*.

$$I_{POA_{dif,reflect}} = GHI\sigma_a \frac{1 - \cos\beta}{2} \quad (7)$$

Where σ_a is the albedo, set at 0.25 following the PV-lib assumption [42]. Equation *(8)*, was used to estimate the $I_{POA_{dif,sky}}$.

$$I_{POA_{dif,sky}} = DHI \times \left[\alpha_i \cos\theta + (1-\alpha_i)\left(\frac{1+cost(\beta)}{2}\right)\left(1 + \sqrt{\frac{DNI \times \cos\theta_z}{GHI}}\sin^3\left(\frac{\beta}{2}\right)\right)\right] \quad (8)$$

Where α_i is the anisotropy index and was calculated by $\alpha_i = \frac{DNI}{DNI_{extra}}$. For this thesis the mean of DNI_{extra} was used to calculate the anisotropy index. The get_extraradiation function in PV Lib [42] was used in Python for this calculation, using the default input. The last term of equation *(8)* was slightly altered in the Python code such that the diffuse irradiance is still computable at night, when the $GHI = 0$, so that the model is able to produce results 0 instead of Not a Number (*NaN*).

III. Solar PV Technical Specification

To accommodate the difference between the urban and rural locations, two different types of configurations and solar PV panels were chosen. Solar farm, where the solar panels are set up in arrays, and solar rooftop, where the solar panels are installed on rooftops.

IV. Rooftop

For rooftop solar, the current most efficient solar panel was used, thereby assuming that this would be the norm in 2030. Currently, this is the SunPower X series: SPR-X22-370 [60,61].

V. Solar-farm

Solar-farm scale project do not necessarily opt for the most efficient solar panels due to the higher costs [62]. Therefore, a utility type solar panel was chosen that has a lower efficiency. It is furthermore important that the PV modules are reliable. The Trinasolar TSM-330PD14 [63], showed to be reliable [64], and was chosen as the utility panel.

VI. Tilt and azimuth

The optimal tilt to maximize production of energy of solar PV panels varies between countries having a range of 32° up to 40°, and does not only depend on the latitude but also on general weather conditions [65]. Consequently, these values were used for solar farm configurations and

can be seen in Table 2-2. For rooftop PV the tilt angle was fixed at 35°, since there was no general data available on the percentage of tilted roofs in the case study area nor how much the angle of these roofs generally is. The chosen angle of 35° was in line with [16,66].

Adjusting the tilt angle due to the shadowing of other buildings, mountains or other objects were not taken into account. The azimuth chosen was 180° degrees south in line with [16,67]. Table 2-2 gives an overview of the angles that are used in this thesis for the solar panels.

Table 2-2: Solar panel azimuth and tilt angles

Type	Country	Azimuth (γ)	Tilt (β)
Rooftop	All	180°	35°
Farm	Belgium	180°	35°
	Germany		32.5°
	Luxembourg		35°
	Norway		40°
	The Netherlands		34°
	Ireland		36°
	Denmark		36°
	United Kingdom		34°

VII. Solar PV model

Various PV array models convert the POA irradiance components to power output exists [68,69]. This thesis used the PVWatts model to calculate the power output per type of panel, $P_{eff,a,t}$, from the POA irradiance and the cell temperature [46,70]. The equation is slightly altered to accommodate additional losses such as inverter efficiency following [16], see *(9)*.

$$P_{eff,a,t} = P_{dc0}\left(\frac{I_{POA_{i,t,x}}}{I_{standard}}\right)\left[1 + \gamma_{pdc,x}\left(T_{cell,a,t} - T_{ref}\right)\right]PR \qquad (9)$$

Where P_{dc0} is the rated power of the solar panel, $I_{standard}$ the reference irradiance of 1000 W/m2, $\gamma_{pdc,x}$ the temperature coefficient of the module, T_{ref} is the reference temperature taken

to be 25 °C, and PR, the performance ratio of the solar cell accounting for efficiency losses. A PR value of 0.9 was chosen following [16,71]. $T_{cell,a,t}$ is the cell temperature and was calculated using the Sandia PV Array Performance Model [72], see (*10*).

$$T_{cell,i,t,x} = I_{POA,a} \times e^{a+b\times u_{10m,i,t}} + T_{i,t} \quad (10)$$

Where a and b are parameter based on the module construction, for each panel they were assumed to be $a = -3.47$, and b = -0.0594 corresponding to an open rack cell glassback solar panel. $u_{10m,i,t}$ is the windspeed at 10m height, taken from the ERA5 data. $T_{i,t}$ is the outdoor temperature, was also taken from the ERA5 database at a height of 2m, and was assumed to be the same for both arrays and solar farms.

The capacity factor, $CF_{a,t}$, was then calculated by *(11)*. Where $P_{dc0,x}$ is the rated power of the panel selected at the site.

$$CF_{a,t} = \frac{P_{eff,a,t}}{P_{dc0,x}} \quad (11)$$

After the CF values were calculated, the two solar PV configurations were merged since no solar farm can be installed at rooftop location and vice versa. The additional benefit was, was that it reduced the computation time.

2.2.2 Wind Power Conversion

The transformation of hourly wind speed data into hourly wind power production is explained in this section. A division is made between onshore and offshore locations. Figure 4 shows the steps taken to perform the conversion.

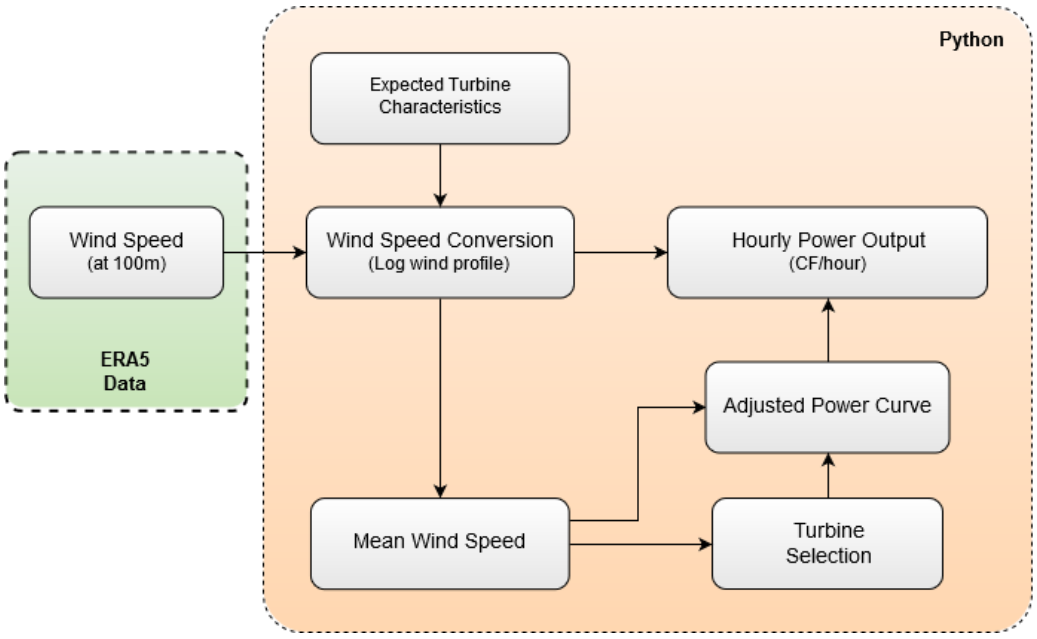

Figure 4: Model outline Wind Power Conversion

The first section describes the expected turbine characteristics that define the hub height of the turbines. In section II, the wind speed conversion is explained. In section III the average wind speed for the time period of 1979-2019 was calculated for each grid cell. Which served as input for the turbine selection at each location. Alternative wind power curves were constructed to incorporate the effect of the position of wind turbines in a wind farm layout in section IV. In section V, the adjusted power curve, the selected turbine per site and the wind speed were converted to the hourly power output. All of these methods were programmed in Python.

I. Expected Turbine Characteristics

Wind turbines are installed either onshore or offshore which results in different technical characteristics [32]. The EEA projected various characteristics, such as hub height, and rated power for both onshore and offshore turbines until 2030 [32]. However, the industry is changing rapidly as 2030 projections for onshore installed turbines are already surpassed [32,73]. Therefore, the used specifications are outlined below and can be seen in Table 2-3.

Onshore

In 2018, Norway has installed onshore wind turbines with an average power rating of 3.6 MW, with a 2.7 MW average in Europe [73]. In 2015, the rotor diameter on average is 100 m and the hub height is 85 m (increasing by 9% in 11 years) [74]. Meaning that the assumption from EEA do not hold anymore. This thesis assumed a hub height of 100m, and the average rated power will be used as an indication to select the onshore turbines.

Offshore

Currently, for offshore turbine, the average rated capacity is 6.8 MW [73], below the EEA assumptions of 10 MW [32]. In 2015, rotor diameter is 115 m and increased 1.6 times 2006. The hub height of 87 m [74] is again below the numbers of the EEA, which states a hub height of150 m and rotor diameter of 120 m respectively. For offshore locations the projections of the EEA still hold and were used in this thesis.

To summarize, Table 2-3 presents the specifications that are used as an indication for choosing the specific wind turbine types.

Table 2-3: Turbine specifications used for selecting turbine

	Rated power (MW)	Hub height(m)
Offshore turbine	10	100
Onshore turbine	3.6	120

II. Wind speed conversion

The ERA5 wind speed data was taken at 100m above ground and needs to be changed to accommodate for the change in height for offshore turbines. The initial data gave the wind speed in two vectors and were combined to one value. The wind speed, u, depending on height, h, was calculated from ERA5 data using the wind speed log equation, (*12*), following [75–77].

$$u = u_s \frac{\ln\left(\frac{h-d}{z_0}\right)}{\ln\left(\frac{h_s-d}{z_0}\right)} \qquad (12)$$

Where h_s is height at 100m and $u_s$the windspeed at h_s. z_0 is the surface roughness length and d the displacement height. This thesis uses a $z_0 = 0.03$ for available land and $z_0 = 0.0001$ for water [78], in line with [16]. The displacement height is the height where the effect of ground objects on the wind speed starts to wear off and where the wind speed can be taken as 0 [77]. This thesis, however, almost excluded all installation of wind turbines in cities and nature reserves. It is therefore assumed that the displacement height is zero. Equation (*14*) was used to calculate the wind speed at 120m.

III. Mean wind speed

The average wind speed at the two different hub heights was calculated to determine the mean wind speed at hub height for the period of 1979-2019. The mean wind speed together with the expected wind onshore rated capacity, see Table 2-3, was used to determine what onshore turbine is used. First, the turbines were selected based on their rated power. Second, the mean wind speed was used to identify the turbine type (I, II, & III), per location based on the approach by the International Electrotechnical Commission (IEC), see Table 2-4.

The average wind speed is not used for offshore locations where wind turbines of IEC class S are used [79]. The power curves from the turbines in Table 2-4 were used to compute the altered power curves.

Table 2-4: Wind speed classes

Wind speed class	**Average wind speed (m s^{-1}) (upper limit)** [79]	**Turbine**
I	10	Vestas V112-3.45 [80]
II	8.5	Vestas V126-3.45 [81]
III	7.5	Vestas V136-3.45 [82]
S	Not applicable	MHI Vestas V164-9500 [83]

IV. Adjusted power curve

The spacing of the wind turbines in this thesis was set at 10D downwind, 5d crosswind based on [84,85]. Due to the spatial resolution of the weather data it was assumed that the wind turbines were placed in wind farm formation. To account for placing the wind turbines together, a multi-turbine model was used to smoothen the power curves [2]. This model takes into account the memory effect of wind turbines on the average wind, by block averaging the original wind speed time series. However, since the spatial resolution and time step of the ERA5 data is high compared to the studies data [2], the differences between the original wind speed data and the new wind speed data were only minimal. Therefore, the original wind speed time series was used to calculate the power output.

The power curves were adjusted to mimic a multi turbine layout, following the method outlined in [2]. This method was not performed for each location, i, but for one offshore grid cell and one onshore grid cell to reduce computation time. The locations can be seen in Table 2-5.

Table 2-5: Reference locations for multi-turbine method

	Onshore	Offshore
Location (latitude, longitude)	52.0/6.75	53.0/3.5

Assuming a turbulence intensity of 0.075 following [86], and an area dimension of the ERA5 area, ~28 km by ~28 km, the normalised standard deviation, σ_n, is equal to 0.05 [2]. The actual wind standard deviation according to [2], σ_w is equal to multiplying σ_n with u_{avg}. The results can be seen in Table 2-6.

Table 2-6: Average wind speed and standard deviation for offshore and onshore location

	Onshore	Offshore
$\boldsymbol{u_{avg}(m/s)}$	6.30	9.69
$\boldsymbol{\sigma_w}$	0.315	0.485

A normal distribution is generated for these locations putting in σ_w in *(13)*.

$$f(k) = \frac{1}{\sqrt{2\pi\sigma_w^2}} e^{-\frac{k^2}{2\sigma_w^2}} \quad (13)$$

Where k is the wind speed offset. ps, the probability distribution was calculated by integrating over $f(x)$. The multi turbine power curve, Pm_q was consequently computed using *(14)*.

$$Pm_q = \sum_q Ps_q \times ps \quad (14)$$

Where Ps_q is the discrete single turbine power curve element. This leads to the power curve that is shown in Figure 5. For each turbine a new multi turbine power curve was made.

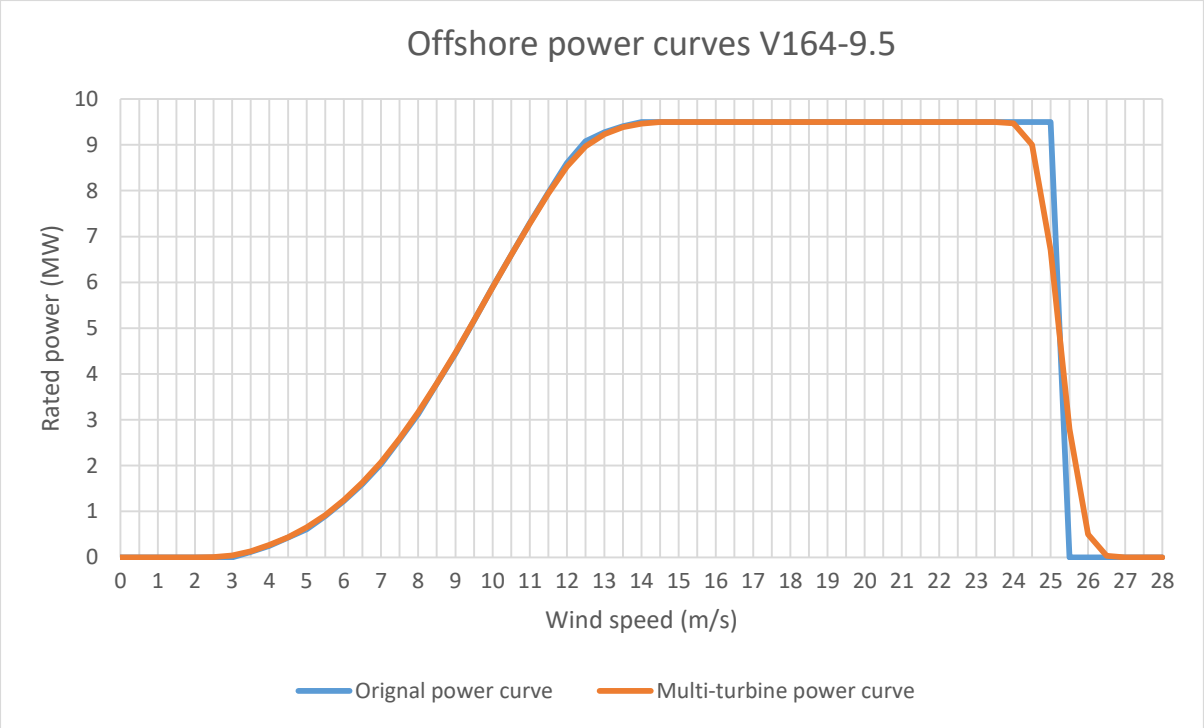

Figure 5: Offshore original and multi-turbine power curve

V. Wind turbine power output

This multi-turbine power curve together with the adjusted wind speed made it possible to calculate the power output per grid cell per time, $P_{i,t,x}$. The Python function power_curve out of the windpowerlib Python library was used for this step [87].

Additionally, wake and availability efficiencies were used to finalize the calculation. The output of wind turbines in a wind farm influence each other, referred to as array efficiency or wake effect [32]. There is a discrepancy in literature on the value used to accommodate for wake losses

[16,23,32,75,88,89]. This thesis used a wake effect, η_{wake}, of 10% for offshore turbines and 7.5% for onshore turbines in line with [32]. The availability of the turbines, η_{avail}, is decreased due to maintenance periods and power outages, this thesis used 5.5% for both offshore and onshore locations in line with [90]. The effective power output per location per time point was thus computed with *(15)* in line with [89].

$$P_{eff\ a,t} = \eta_{wake}\eta_{avail}P_{a,t} \qquad (15)$$

Where $P(t)$ is the power output at each time point, t, and location, i. The capacity factor was determined using *(11)*. The capacity factor, CF, was calculated using equation (*16*).

$$CF_{a,t} = \frac{P_{eff\ a,t}}{P_{rated}} \qquad (16)$$

2.3 Capacity Constraint

The next section describes the methods used to determine the maximum installable capacity of solar and wind power per grid cell, see Figure 6. The first subsection explains the determination of the usable area. The second and third subsections explain how to determine the maximum power density of solar and wind power, respectively. The final subsection combines the usable area and the power density to form the maximum power potential per grid cell.

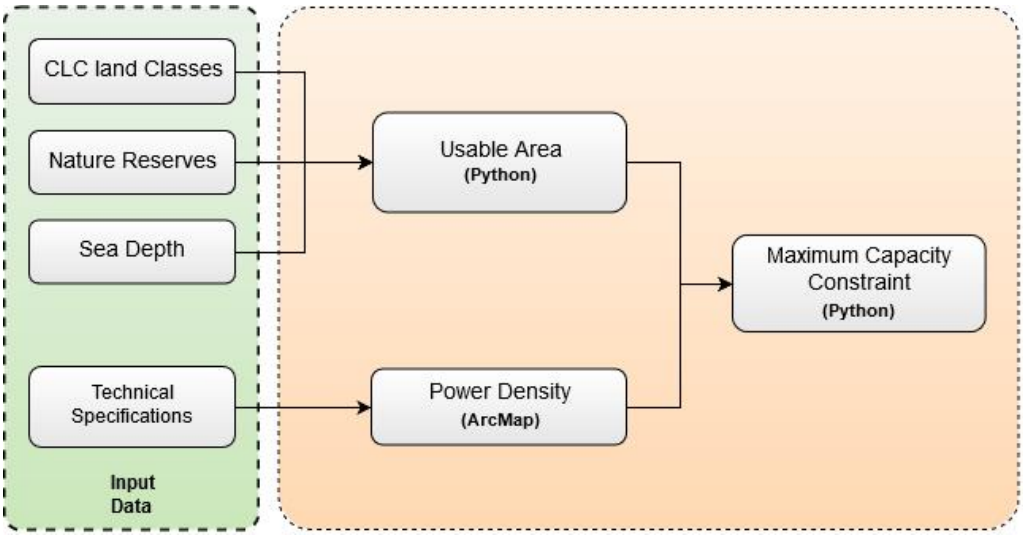

Figure 6: Flow chart maximum capacity constraint

2.3.1 Usable area

The area available, A_{avail}, for the production of renewable electricity was limited by a multitude of factors, such as urban areas and nature reserves [91]. This reduction in land availability was approximated by the suitability factor, f_i, for each location of i, and technology x, inspired by [91]. f_i resulted from combining the suitability variables, a_i, b_i and ω_i in a high-resolution map per technology. Where a_i, is the area weighting, w_i, is the suitability factor regarding land cover and b_i is the suitability factor for nature reserves. This map was consequently resampled to the right resolution using bilinear interpolation option in the ARCGIS tool [92]. The initial combination was possible as the different suitability values did not geographically overlap at high resolution. All of the variables were set at a range of 0, meaning the area cannot be used, to a 100, where the area can be fully used.

Following the report by the European Environmental Agency, protected nature reserves are classified as Natura 2000 areas and Common Database on Designated area sites [32]. In these areas $b_i = 1$, this is used because wind turbines have been shown to be installed in these areas in the region selected by this study [93], but these areas still fall under protection [32]. The files were downloaded from [94,95].

Corine Land Cover (CLC) definitions [96], were used to determine the area weighting, ω_i. The CLC land types picked for each technology are given in Table A-i. Only buildings in the urban fabric class are assumed to be able to install solar rooftop. Increase in population, from 2018-2030, and the corresponding increase in urbanized area was not taken. The values of ω_i are given in Table A-ii.

The area weighting, a_i for wind onshore is unlimited by altitude. a_i for offshore refers to the maximum sea depth as floating wind turbines are not considered in this thesis. The depth was set at 50 m, in line with [16,32]. The value ranges from 0 to 100 for each offshore location, where 0 means that the sea is deeper than 50m and 100 means the sea is shallower than 50 m. a_i, for wind offshore, solar farm and solar rooftop configuration was set at a 100.

An overview of the suitability variables and their range for each technology is given in Table 2-7.

Table 2-7: Suitability variables and their references, the range is 0-100

Variable	Wind onshore	Wind offshore	Solar PV Rooftop	Solar Utility
a_i	100	0 or 100	100	100
ω_i, see Table A-ii	Specified values [91]	100	Specified values [16]	Specified values [91,97]
b_i	100	100	100	100

2.3.2 Solar PV power density

Assuming the tilt for solar rooftop outlined in section 2.2.1.VI, the area used for these solar panels is higher than the building's footprint, following Pythagoras's theorem. The used tilted area, A_{used_tilted} for solar rooftop is 1.22 m² per m² roof, under the used tilt value of 35°. Other limiting factors such as chimneys or roof terraces were not taken into account. The used area for rooftop PV, $A_{used,x}$, per solar panel horizontally is calculated using (*17*), where $A_{panel,x}$ is the area of the panel.

$$A_{used,x} = \frac{A_{panel,x}}{A_{used\_tilted}} \tag{17}$$

The A_{used}, for one panel in a solar farm is calculated using *(18)* following [98].

$$A_{used,i,x} = A_{panel,x}\left(\cos\beta + \cos(\gamma_{ref} - \gamma)\frac{\sin\beta_i}{\tan\alpha_{ref}}\right) \tag{18}$$

Where A_{array} is the area of one panel, β_i, the tilt of the panels per country, γ_{ref}, the reference solar azimuth angle, and α_s the solar altitude angle calculated by $\alpha_{ref} = 90° - \theta_{z,ref}$. $\theta_{z,ref}$is the reference zenith angle. For all solar locations the assumption is made that the solar altitude angle is 14° and the solar reference azimuth is 179° [99], following the location of Berlin at winter solstice of 21 December 2016, in line with [16]. This stands in contrast with other methods that estimate the solar altitude angle either at 10:00 or 14:00 at winter solstice [98]. However, since

this leads to unrealistic high values for A_{used} for array operation in especially Norway, this approach was not adopted.

The maximum power density, $\hat{p}_{x,i}$, per technology x, in location i,is calculated using (*19*).

$$\hat{p}_{x,i} = \frac{P_{dc0,x}}{A_{used,i}} \quad (19)$$

Where $P_{dc0,x}$ is the rated power of the solar panel. The values of A_{used} and $\hat{p}_x$for both rooftop and solar farm can be seen in Table 2-8. The values are considerably higher compared to the wind turbine power densities, see Table 2-9. This high estimation is based on the maximum power production and assuming that the whole area can be build full of solar panels. This value is further restricted by the usable area which result in the maximum capacity constraint, see section 2.3.4.

Table 2-8: A_{used} and maximum power density for solar panels

Type	Country	A_{used} (m²/panel)	$\hat{p}_x$ (MW/km²)
Rooftop	All	1.4	235.7
Farm	Germany	5.8	63.8
	Norway	6.5	56.9
	United Kingdom	6.0	61.7
	Netherlands	6.0	61.7
	Belgium	6.1	60.7
	Luxembourg	6.1	60.7
	Ireland	6.2	59.7
	Denmark	6.2	59.7

2.3.3 Wind power density

The power density of wind turbines was determined using their rotor diameter. For offshore locations, one power density value was calculated and for onshore locations 3 power densities were calculated matching the different diameters for each turbine. For all locations a wind turbine spacing of 10D downwind and 5d crosswind was used [85]. The maximum power densities, $\hat{p}_x$, per technology, x, is given by *(20)*.

$$\hat{p}_x = \frac{Pr_x}{10D_x \times 5D_x} \quad (20)$$

Where Pr_x is the rated turbine power. The values of $\hat{p}_x$ are given in Table 2-9.

Table 2-9: Power densities per wind turbine

Turbine	Power Density (MW/km²)
V112-3.45	5.13
V126-3.45	4.35
V136-3.45	3.73
V164-9.5 (offshore)	7.06

The power density of the offshore turbine is higher than that of current wind farms [100]. However, all values are below the assumed power density values in [32], and are therefore conservative estimates. The different power densities were combined in one map. The selection of them depended on the average wind speed of that grid cell following the IEC approach [79]. The values were consequently used to determine the maximum potential per grid cell.

2.3.4 Maximum capacity constraint

The result of the above mentioned approach yielded 4 suitability maps and 4 power density maps, one for each technology. They were used for the maximum power constraints, $c_{x,i}^{max}$, per grid cell, i, and technology, x. This combination was done using *(21)*.

$$c_{x,i}^{max} = f_{x,i} \times \hat{p}_{x,i} \quad (21)$$

Where $f_{x,i}$, is the suitability factor, for each technology x and location i calculated in section 2.3.1. $c_{i,x}^{max}$, was set as a limit for the maximum allowable power per technology per location.

2.4 Expected installed capacity

The total installed capacity per technology per country in 2030 was used as a constraint in the model. For onshore and offshore wind power the WindPower Europe projections for the Central

Scenario were used [101], with the exception of Norway offshore due to the lack of data. The combined expected installed capacity for solar total was used and was based on [102]. Here too Norway was not included in the data.

For Norway, the expected installed capacity for offshore wind and solar total was derived from [103] and was converted to installed capacity using a capacity factor of 32.6% for wind offshore [104] and 13% for solar total [105]. The resulting expected installed capacity values can be seen in Table 2-10. The total installed VRE capacity, ca_{VRE} (solar + wind) is 277.295 GW.

Table 2-10: Expected installed capacity in 2030

Country	Onshore wind (MW) [101]	Offshore wind (MW) [101]	Solar Total (MW) [102]
Norway	10000	10 310 [103]	4 391 [103]
Denmark	5 000	4 300	838
Germany	70 000	15 000	63 959
The Netherlands	8 000	11 500	5 586
United Kingdom	15 000	22 500	11 043
Ireland	5 600	1 800	19
Belgium	4 400	4 000	3 818
Luxembourg	100	0	131
Region	118 100	69 410	89 785

2.5 Electricity demand

The hourly electricity demand was taken from [26,106] at national resolution. The data ranges from 2010 to 2019 for the countries in the region under study. Adjustments to the data set were made so that the whole data set was set in one time-zone. For details see Appendix B.

The hourly demand data, $E_{t,country}$, was adjusted to account for a changing electricity demand in 2030, see *(22)*.

$$E_{t,2030,\text{country}} = E_{t,country} \times \alpha_{\text{year,country}} \quad (22)$$

Where $E_{t,2030,\text{country}}$ is the adjusted electricity demand for $country$ at each hour and $\alpha_{year,\text{country}}$ is the expected increase in demand from $year$ up to 2030. $\alpha_{year,\text{country}}$ was calculated using (*23*).

$$\alpha_{year,country} = \frac{E_{2030,country}}{\sum_{t=1}^{year} E_{t,country}} \quad (23)$$

Where $E_{2030,country}$ is the expected annual energy demand of $country$ in 2030 and $\sum_{t=1}^{year} E_{t,country}$ is the summed annual energy demand of $country$ in $year$. $E_{2030,country}$was based on the EU projections of 2030 taken from [107]. To conclude, the hourly adjusted energy demand was normalized using min-max normalization, see (*24*).

$$d = \frac{d_e - \min(d_e)}{\max(d_e) - \min(d_e)} \quad (24)$$

Where d_e is the original electricity demand and d is the normalized electricity demand with a range from $0 - 1$.

2.6 Portfolio Analysis

The Mean Covariance Analysis (MCVA), was performed twice. First, the model was performed loosely constrained, where the total sum of the expected VRE capacity was set as the installation constraint. Secondly, the constrained scenario sets the maximum installed capacity of each VRE technology equal to the country's expected installed capacity shown in Table 2-10. The portfolio optimization was performed in R Studio, drawing inspiration from [14,108].

The portfolio optimization for MCVA aimed to maximize the covariance between the VRE production and the energy demand, $Cov(r_p, d)$. The MCVA is an optimization problem and was formulated by (*25*). The optimization is subjected to the constraint where the weights of all assets, w_a, should be equal to 1, and the weights of the assets should be smaller than their maximum potential divided by the expected installed VRE capacity. For the constrained optimization the sum of the weights of each asset should be bigger or equal to the expected installed VRE capacity

per technology for each country, ca_a, over the total region's expected capacity. r_p are the return CF values of the portfolio and d is the normalized demand data.

$$\max_{w_a} Cov(r_p, d) \quad \text{subject to} \begin{cases} \sum_a w_a = 1 \\ w_a \leq \frac{c_a^{max}}{ca_{VRE}} \\ constrained \left(\sum_a w_a \geq \frac{ca_a}{ca_{VRE}} \right) \end{cases} \tag{25}$$

To complete the optimization problem in *R,* the covariance was rewritten in matrix notation, see *(26)*.

$$Cov(r_p, d) = Cov\left(\sum_{a=1}^{n} w_a r_a, d\right) = \boldsymbol{cov^T}(\boldsymbol{r_a}, \boldsymbol{d}) \cdot \boldsymbol{w} \tag{26}$$

Where $Cov(r_p, d)$ is the covariance between the energy demand, d, and the portfolio output, r_p. n is the total number of assets, and r_a the return of asset a. The MCVA is a linear optimization problem instead of a quadratic optimization problem, due to its one weight vector. To perform the optimization the covariance was rewritten in matrix notation see *(26)*, where $\boldsymbol{cov^T}(\boldsymbol{r_a}, \boldsymbol{d})$ is the transpose covariance matrix and $\boldsymbol{w}$ is the weight matrix of weights w_a.

To create the efficient frontier, the optimization started with calculating the portfolio with the highest return, μ_p. μ_p is first rewritten to matrix notation, see *(27)*.

$$\mu_p = \sum_a w_a \mu = \boldsymbol{\mu^T w} \tag{27}$$

Where $\boldsymbol{\mu^T}$, is the expected return vector of all assets a. The first linear optimization maximized μ_p, while conforming to the constraints set in *(25)*. The second optimization set to maximize the covariance, thus solving (*25*). These two optimizations yielded 2 portfolios, one with the highest return and one with the highest covariance.

The next step in creating the efficient frontier was to determine the return of 48 portfolios between the maximum covariance portfolio and the maximum return portfolio using linear interpolation. For each of these 48 returns the covariance was consequently minimized. Together, the return and covariance of these 50 points produced the efficient frontier.

After the unconstrained optimization of MCVA, the constrained optimization was performed. The constraints for each technology were first converted to maps in ArcGIS so that they could be loaded into R Studio. This constrained optimization led to the second set of efficient frontiers.

2.7 Demand Response

The DR optimization was performed in Python using the Gurobi optimization software [109], because it is both relatively fast in operation and free to use for academic purposes [109,110]. The demand response optimization was performed on the constrained scenario because this scenario more accurately presents reality as countries have their own VRE targets.

DR for both industry and the residential sector is season sensitive [11,111]. Furthermore, the frequency with which the demand response can be initiated differentiates across technologies [11,27]. In other studies, the demand in DR is shifted to a maximum of 24 hours which depends on the chosen technology [11,27,31,111]. In this thesis it was assumed that the DR potential lasts 12 hours meaning that the DR added or subtracted to the demand initially has to be re-used or withdrawn within 12 hours from the initial start of the demand response.

The DR potential used in this study was adapted from [11]. The minimal theoretic load reduction per country was taken as a percentage of the total peak load from [11]. The percentage was applied to maximum load demand of each country's 9-year demand data. This yielded 8 separate potentials and when added together led to an estimated DR reduction potential of 22.7 GW. This potential was also used for load decrease potential. The potential was set as the maximum allowable DR increase or decrease for a period of 12 hours.

To do this, the maximum return portfolio's electricity production was chosen as the frame of reference for the DR optimization. It was chosen because for this solution the electricity return was maximized, while for the other constrained portfolios on the efficient frontier the demand had an

active role in determining both the covariance and electricity output. To maximize the covariance the slope of the production and the load should be as close to each other as possible. Therefore, the total sum of the difference in the slope should be minimized. This resulted in the optimization problem as formulated in *(27)*.

$$\min \sum_{t=1} \left(\left(r_{p,t} - r_{p,t-1} \right) - \left(\left(d_t + DR_t \right) - \left(d_{t-1} + DR_{t-1} \right) \right) \right)^2 \qquad (28)$$

$$subject\ to \begin{cases} -23 \leq DR_t \leq 23 \\ \sum_{t_{start}}^{t_{start}+12} DR_t = 0 \\ \sum_{t_{start}}^{t_{start}+12} |DR_t| \leq 45.4 \end{cases}$$

Where $r_{p,t}$ is the return of the max return portfolio at time t, d_t is the original demand time series and d_{t-1} is the previous demand time series. DR_t refer to the demand response and used in time t. t_{start} is the time point where the DR is initiated. The last constraint ensures that the DR stays within the limit of 22.7 GW over the whole 12 hours. The constraint uses 45.4 GW because DR can be both negative and positive.

The function to be minimized was squared because Gurobi does not allow for absolute values to be in the objective function. Since squaring would eliminate the negative sign and the minima of this function was not used in this thesis it was chosen as a replacement.

The optimization was performed multiple times where both the duration and the maximum potential was varied from 1/4th the potential to quadruple the potential and 1/4th the duration to quadruple the duration. Varying the output and duration of DR allowed for creating a sensitivity analysis for DR.

2.8 Portfolio Optimization Post Processing

The results were post-processed to gain a better understanding of their implications. The weights of each portfolio were converted back to a coordinate system so that they could more intuitively

used for geographic analysis. The return of the portfolio analysis is the CF of the whole portfolio, this was converted to average annual energy use by using the capacity constraint.

To be able to perform a clearer interpretation of what the covariance of the portfolio's and the energy demand means the covariance was translated into the correlation coefficient ρ_{d,r_p} using (*29*).

$$\rho_{d,p} = \frac{Cov(p,d)}{\sigma_p \times \sigma_d} \tag{29}$$

Where σ_{r_p} is the portfolio's standard deviation, and σ_d is the demand standard deviation. This transforms the scale from $-\infty \leq x \leq \infty$ to $-1 \leq x \leq 1$ making understanding of the results more intuitive as the minimum correlations refers to that the energy demand and portfolio are negatively correlated, the maximum correlations refers to that the energy demand and the portfolio are positively correlated and 0 referring to the fact that the portfolio and energy demand are uncorrelated.

3. Results

The first part of this chapter presents the intermediate results, being the CF values per location for the studied period, the maximum installable capacity under the given suitability factor, and the effect of using DR on the electricity demand. The second part shows the results of the unconstrained portfolio optimization. The third part shows the constrained optimization results. The fourth part shows the effect of including DR on the constrained optimization. The last part compares the difference between the three scenarios; unconstrained, constrained and constrained with DR.

3.1 Capacity Factor and Potentials

The capacity factors of both solar and wind power are presented in Figure 7 and Figure 8 respectively. The CFs were the result of the methodology explained in section 2.2. Both figures show the potential CF of each panel without land restrictions. Figure 7 shows the different CFs over a 9-year period that occur between the two panels. It shows that there is a minimal difference between the mean CF of each panel. This could be attributable to the fact that for the solar farm configuration a different panel is chosen as well as a different tilt angle.

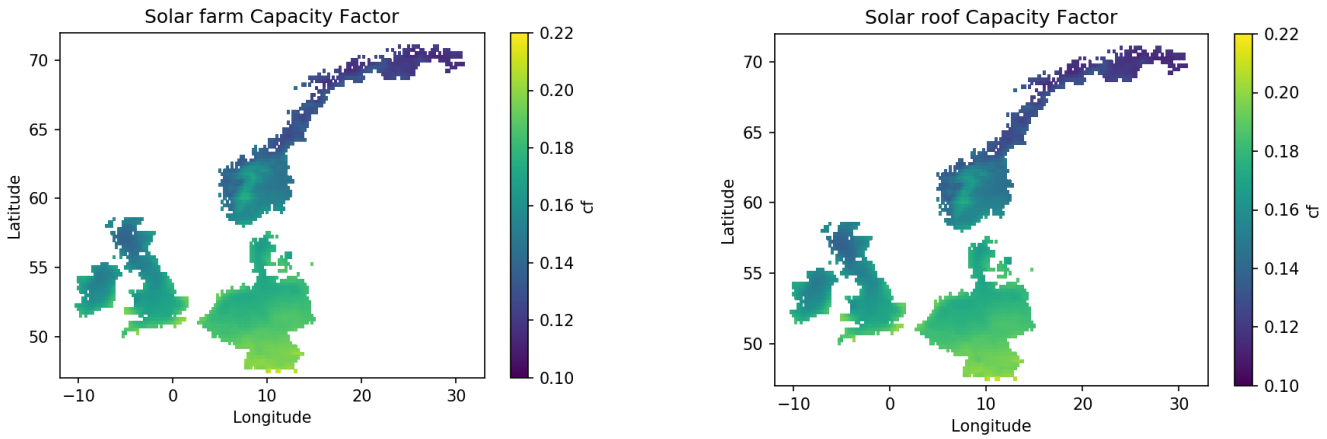

Figure 7: CF of solar farm and solar rooftop for 2010 up to 2019

The CF for both solar configurations is generally higher than found in [71,112]. However, differences could be explained to the higher *PR* value used in this thesis as well as a difference in tilt angle usage.

Figure 8 shows the mean CF of offshore and onshore turbines. For onshore locations it clearly shows that mountainous areas, such as the German Alps as well as the Scandinavian mountains have low performance compared to the flatlands and flat areas close to the sea such as Denmark, coastal Netherlands as well as parts of the United Kingdom. The influence of land and/or mountains continues to be seen in the CF values for wind offshore. This is especially the case for the Norwegian fjords. The most optimal locations for wind offshore in terms of mean CF are shown to be at the Atlantic side and the Norwegian part of the North Sea. Most likely this is due to the lack of neighbouring land and general wind direction that is not coming from land. While a clear difference between the two location types exists in terms of their mean-CF output, it shows that the utilization (CF value) of wind turbines is higher compared to solar panels.

The CF values for wind both on- and offshore found by this thesis generally align with the findings of [23,32,112]. Both show high potential for the North Sea and low potential for mountainous regions such as the German Alps. Coastal Netherlands showed to have a higher potential than in [32] but it is more similar to [112]. The CF for wind offshore and the coastal regions was 0.1 lower compared to [23]. This can be explained as the wind turbine used in [23] is producing faster at its peak power than the wind turbines used in this study.

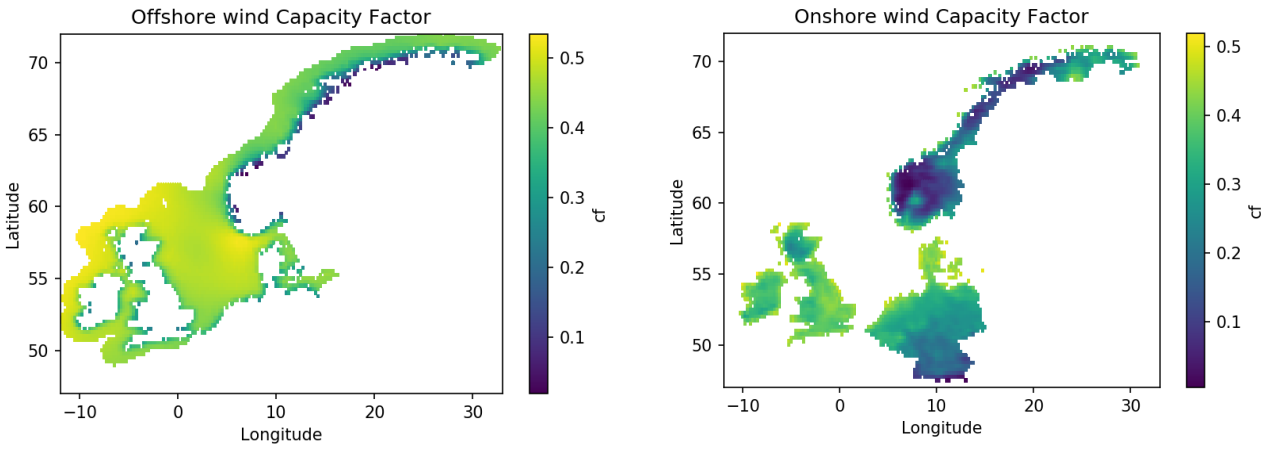

Figure 8: CF of wind offshore and wind onshore for 2010 up to 2019

3.2 Demand Response

The results of the DR optimization run to maximize the constraint's max return portfolio can be seen in Figure 9 and Figure 10. They show the impact of the optimization on the demand. Especially in the winter periods, the evening peak electricity demand has flattened out. When DR is applied during the summer months the daily peak is shifted towards solar noon. Furthermore, the evening demand, form 20:00 onwards, during the summer is higher.

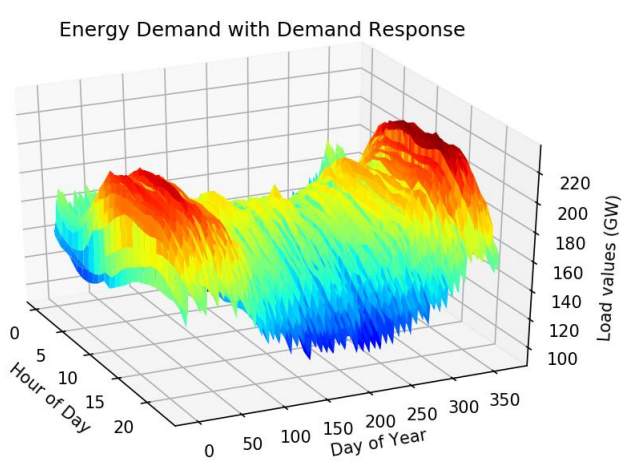

Figure 9: 2010 Electricity demand with demand response, adjusted for 2030 projection

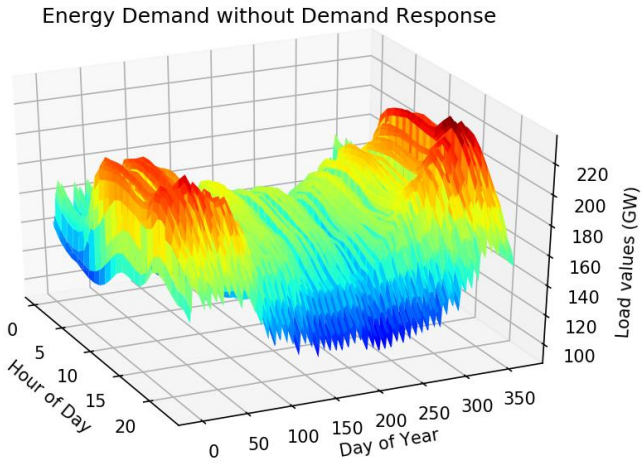

Figure 10: 2010 Electricity demand without demand response, adjusted for 2030 projection

Figure 11, shows this difference more clearly. A positive DR means that demand is added and a negative DR means that demand is subtracted. In the middle of the day DR is mostly positive and during the night while negative in the morning and before the evening starts. This can be attributable to the fact that peak demand mostly occurs in the mornings and the afternoons. Furthermore, solar production is highest during the middle of the day so it is expected that more demand can be fulfilled there.

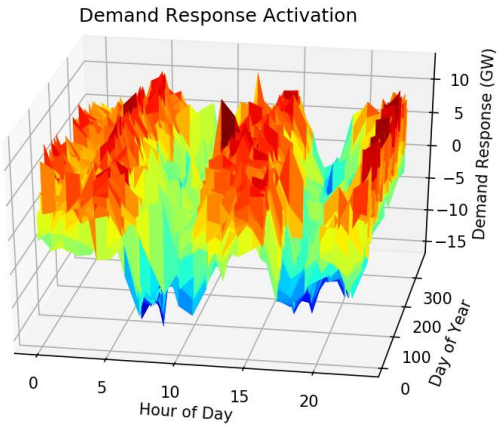

Figure 11: Demand response activation for 2010, adjusted for 2030

3.3 Unconstrained optimization

The efficient frontier for the unconstrained covariance analysis, see Figure 12, shows that there is a clear trade-off between the return of the portfolio's and the covariance between the portfolio and the region's energy demand. The first part of the graph, between a covariance of 0.0056 and 0.008, shows that accepting slightly lower return increases the covariance considerably. The last part of the efficient frontier, between a covariance of 0.0085 and 0.0087, shows that there is more of a trade-off between the return and covariance.

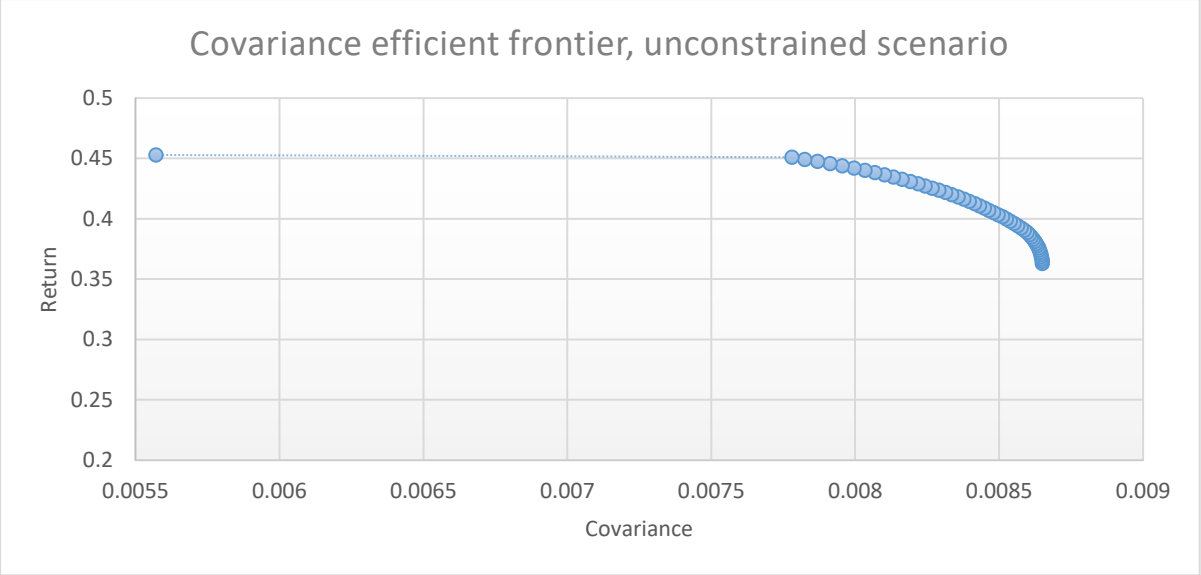

Figure 12: Efficient Frontier Unconstrained covariance analysis

The return-correlation coefficient graph, which uses the results of the covariance optimization, paints a slightly different picture, see Figure 13. While the majority of the graph follows the same trend as the covariance efficient frontier, it is more uneven. This shows that the correlation between energy demand and the portfolio does not exactly follow the same trend as the covariance between the energy demand and the portfolio's return. Especially towards the end of the graph it becomes clear that there is not a 1:1 relationship, as the maximum covariance point does not align with the maximum correlation point for this portfolio.

Nevertheless, it shows that to maximize the correlation between renewable generation and electricity demand, some return has to be given up. In the beginning a return sacrifice (decrease in energy production) of 0.002 increases the correlation by 6%, and might therefore be useful. After this, considerable more return has to be given up to increase the correlation. From the maximum correlation point there are fluctuations in both output and return that do not increase the correlation but do decrease the return. The fluctuation of the correlation graph is attributable to the standard deviation of the portfolios output, which has to change in order to accommodate maximizing the covariance. This variation occurs since the covariance follows a clear trend and the standard deviation of the demand is constant, thus leaving the portfolio's standard deviation as the variable that leads to the deviation in correlation.

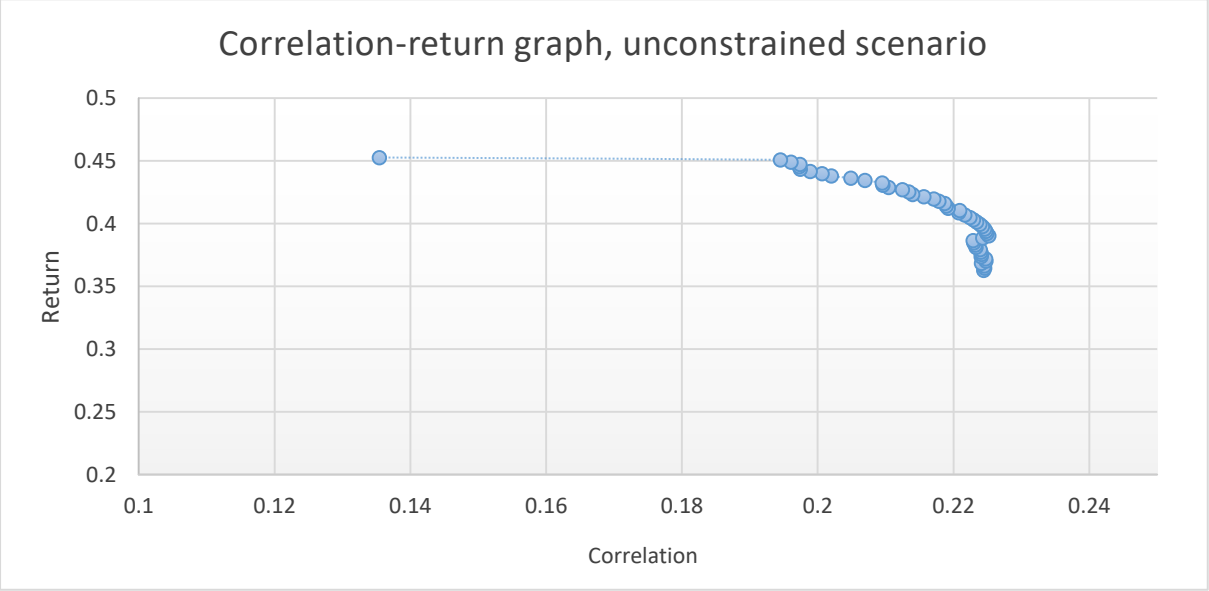

Figure 13: Correlation-Return graph unconstrained scenario

The locations of both the max return portfolio and the max covariance portfolio can be seen in Figure 14 and Figure 15 respectively. The location analysis shows that there are no locations of solar PV installed in the portfolios along the efficient frontier. This can be attributable to the overall lower CF's of solar PV since this scenario aims to maximize return or maximize covariance under maximum possible return.

The locations and installed capacity of wind offshore and onshore for the max return portfolio can be seen in Figure 15. It shows that most of the asset locations are offshore locations in front of the Danish coast and close to Scotland. The vast installation of wind offshore stands in contrast with the few wind onshore locations. These are either on islands or near the coast. This can be explained as the mean CF value of wind offshore turbines is higher than that of wind onshore.

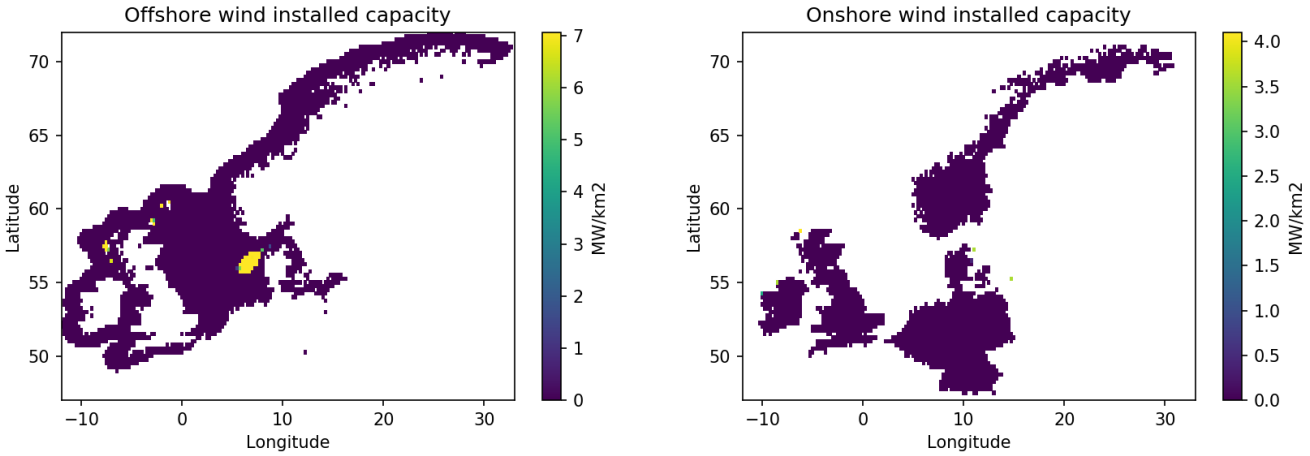

Figure 14: Max-return asset locations and installed capacities for the unconstrained scenario

For the maximum covariance portfolio, see Figure 15. There is a major switch from wind offshore to wind onshore. The asset locations are mostly concentrated in Northern Norway and North-East Scotland. For wind onshore there are only farms installed near the cost of Scotland and middle Norway. It shows that picking wind onshore locations increases the covariance between the return and the electricity demand.

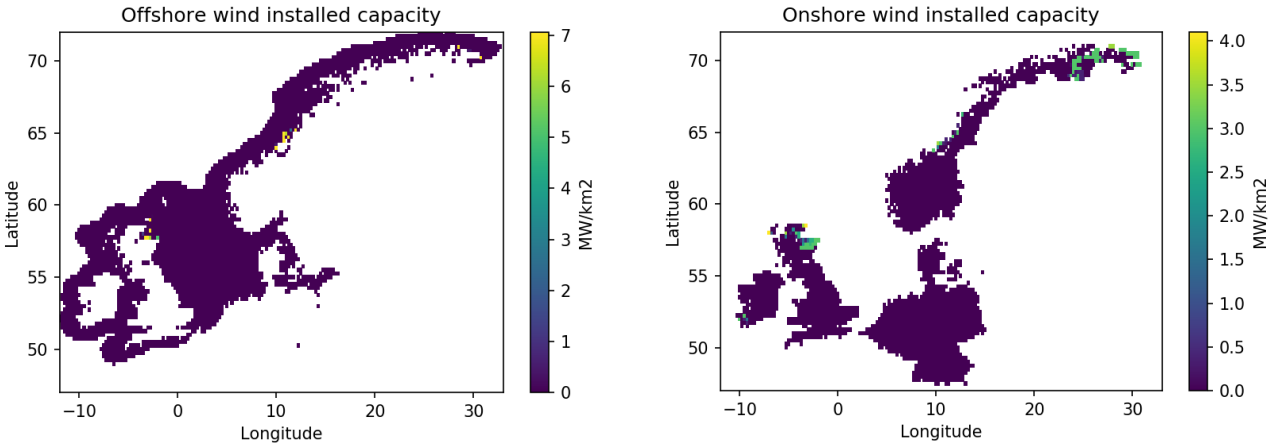

Figure 15: Max-covariance asset locations and installed capacities for the unconstrained scenario

This trend can also be seen in Figure 16, as the times locations are chosen for wind installation for the portfolios on the efficient frontier are shown. The figures indicate that especially in northern Scotland and north Norway exhibit high favourability for the installation of wind onshore. For wind offshore the locations are also in the middle of Norway and the northeast coast of Scotland.

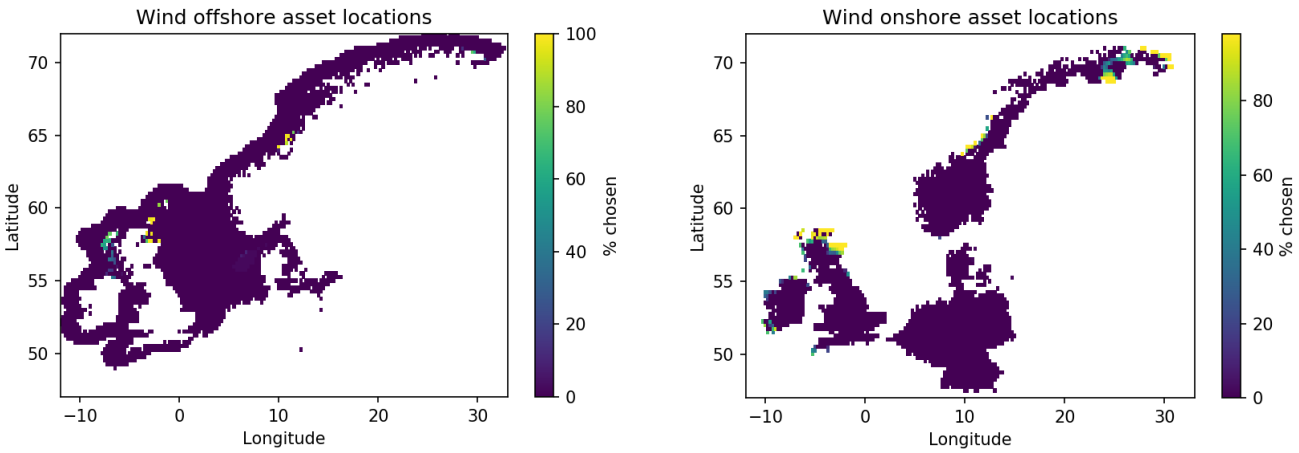

Figure 16: Percentage of locations chosen for portfolios on the efficient frontier, unconstrained scenario

3.4 Constrained optimization

The efficient frontier of the constrained covariance optimization can be seen in Figure 17. It shows that also in the constrained scenario a clear trade-off between the return of the portfolios and the covariance exists. It could especially be beneficial to sacrifice some of the energy return for an increase in covariance, especially where the portfolio's return is around 0.36 as the covariance can be increased by 10 %.

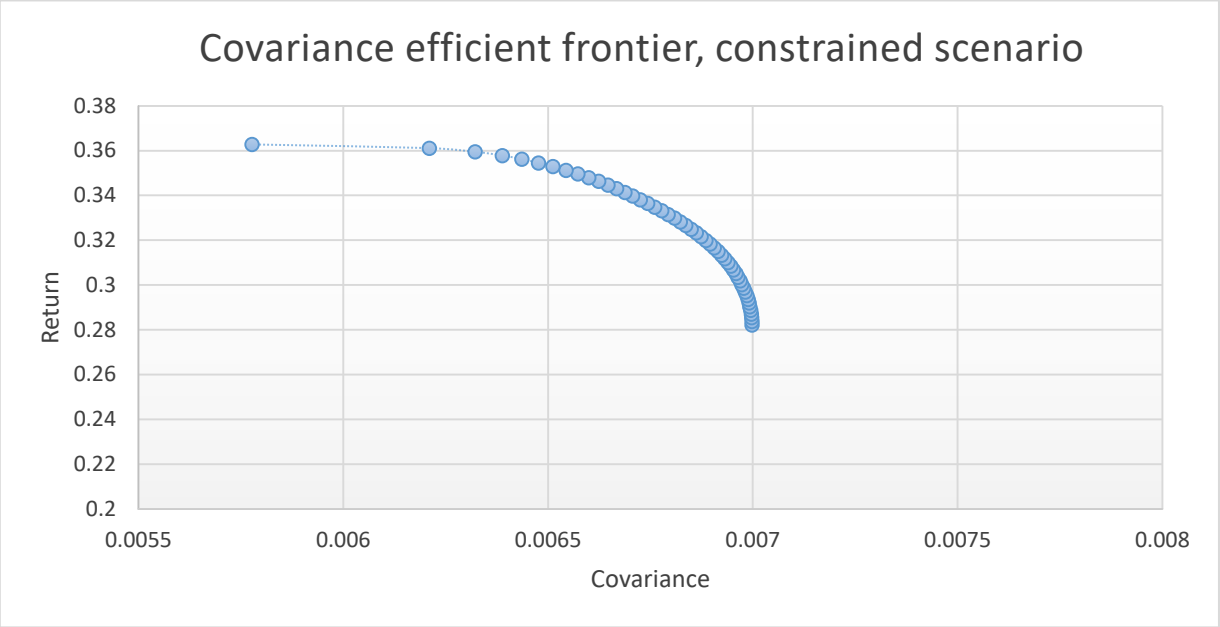

Figure 17: Constrained efficient frontier of the covariance and Return

However, to get a better understanding of what exactly the trade-off is, the correlation coefficient versus the maximum return in the constrained optimization is plotted, see Figure 18. This shows that while the covariance between the energy demand and return of the portfolio follows a clear curve, this is not the case for the correlation- return graph, which is similar in form to Figure 13 the unconstrained scenario. Especially at the point where the covariance is maximized there are a lot of fluctuations. The general trends between the efficient frontier of the covariance-return plot and the plot of the correlation coefficient versus return are however similar. For both graphs, at first less return needs to be sacrificed for an increase in covariance/correlation and later more return has to be sacrificed in order to get the same level of increase in covariance/correlation.

Figure 18 shows that in the first part of the graph, where the return decreases from 0.365 to 0.35, the correlation increases with 4 %. Therefore, in the beginning where the return is around 0.36 it is noteworthy to look into placing the assets in different locations. Especially when aiming to maximize the covariance/correlation a high variation can be seen in the portfolio's return. Slight deviations in correlation can thus drastically influence the return.

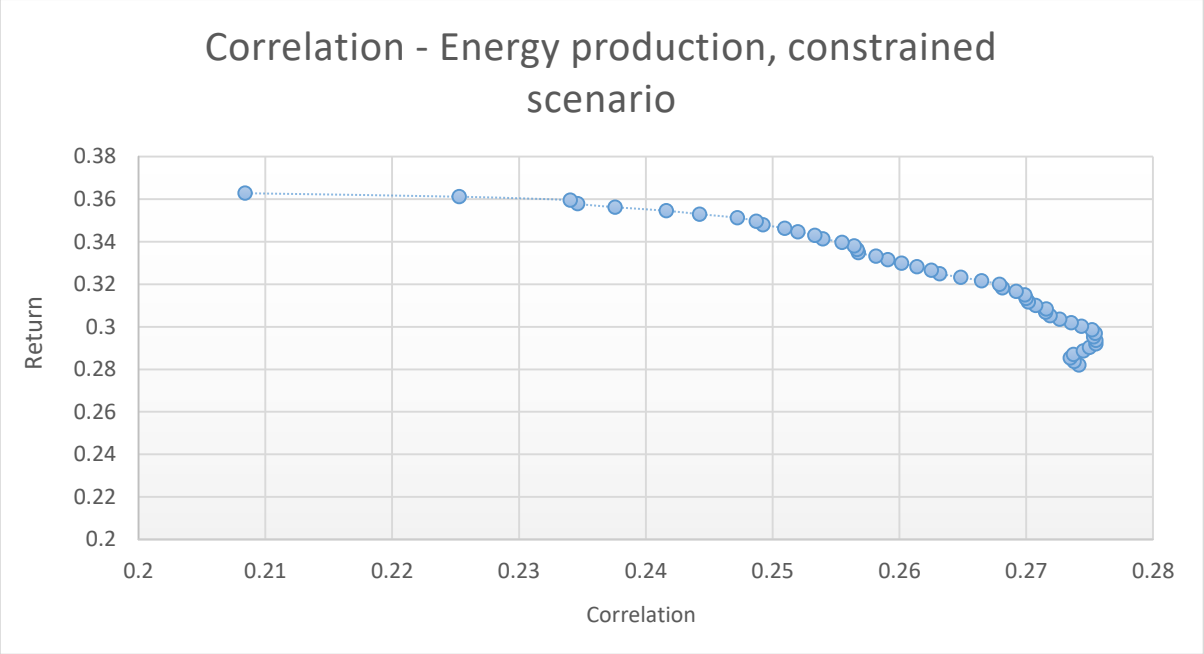

Figure 18: Correlation-Return graph constrained scenario

Figure 19 shows the areas that have the maximum return for the constrained case. It shows that, when maximizing the return, the locations are dispersed using a high share of their maximum installable capacity in the case of offshore wind and solar PV. For the wind onshore there is more variation, especially in the middle of Germany. Solar PV is also geographically dispersed as it is spread out across high irradiance regions.

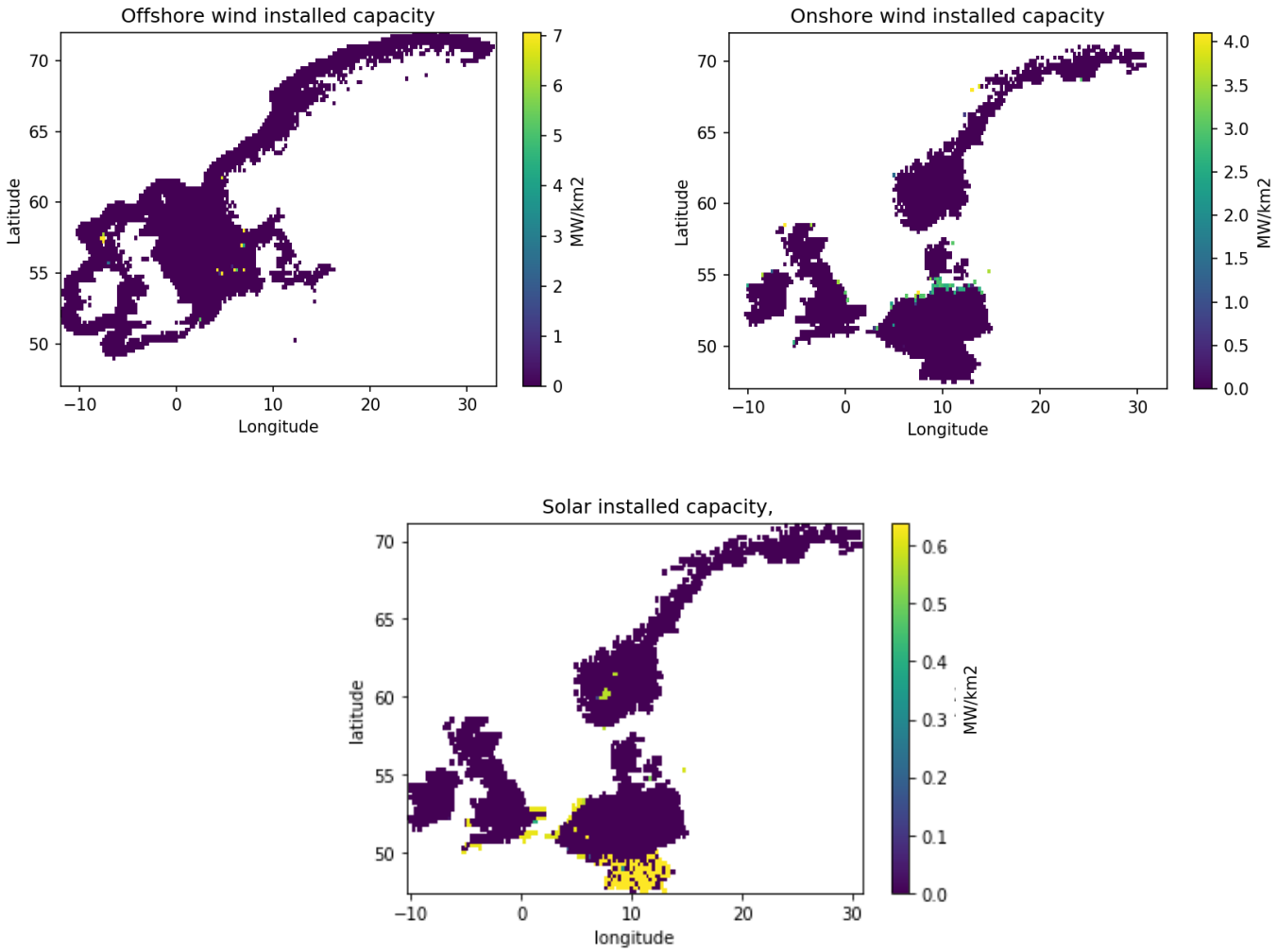

Figure 19: Max-return asset locations and installed capacities for the constrained scenario.

Comparing the max-return portfolio to the max covariance portfolio shows that there is a big difference across all technologies, see Figure 20. Solar PV is plotted twice but with different a different index. The unlimited graph shows that there are a couple of locations where a lot of solar PV is installed. Due to scaling, the locations with a relative lower installed capacity become invisible and the limit graph shows this.

Especially the installation of solar PV locations as they are more concentrated now, especially for Germany. This shift can be attributable to the difference in optimization, maximizing covariance versus maximizing return.

Wind onshore also changes in its locations as they move from northern Germany in the max-return portfolio to central Germany in the max-covariance portfolio. Thereby moving to lower CF zones.

Like the onshore wind locations, the offshore wind locations also move to lower CF regions from places around the Outer Hebrides.

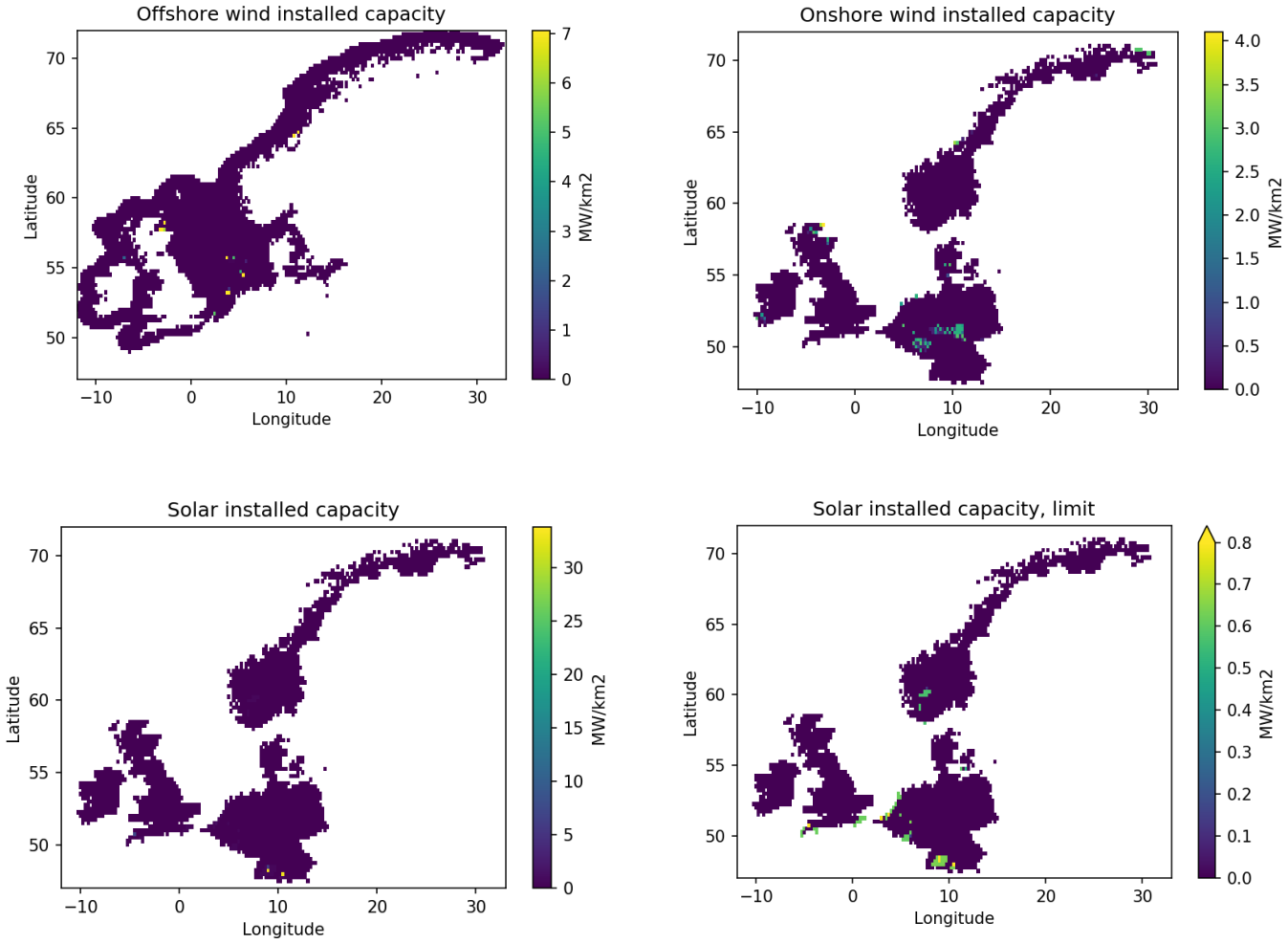

Figure 20: Max-covariance asset locations and installed capacities for the constrained scenario. Solar installed capacity limit refers to a rescaling of the map such that lower installed capacity locations become visible.

The maps in **Figure 20** shows that there is variation in the way the locations are picked for the constrained covariance optimization. To get a better understanding of these dynamics the locations of all the 50 portfolios are mapped in Figure 21. This shows the robustness of installing wind onshore in Scotland, the Dutch coast, Luxembourg and middle Germany, the middle part of the North Sea for wind offshore. For solar PV,the areas of more installation stability are southwest Germany, coastal Belgium and the Netherlands, the UK and central Norway.

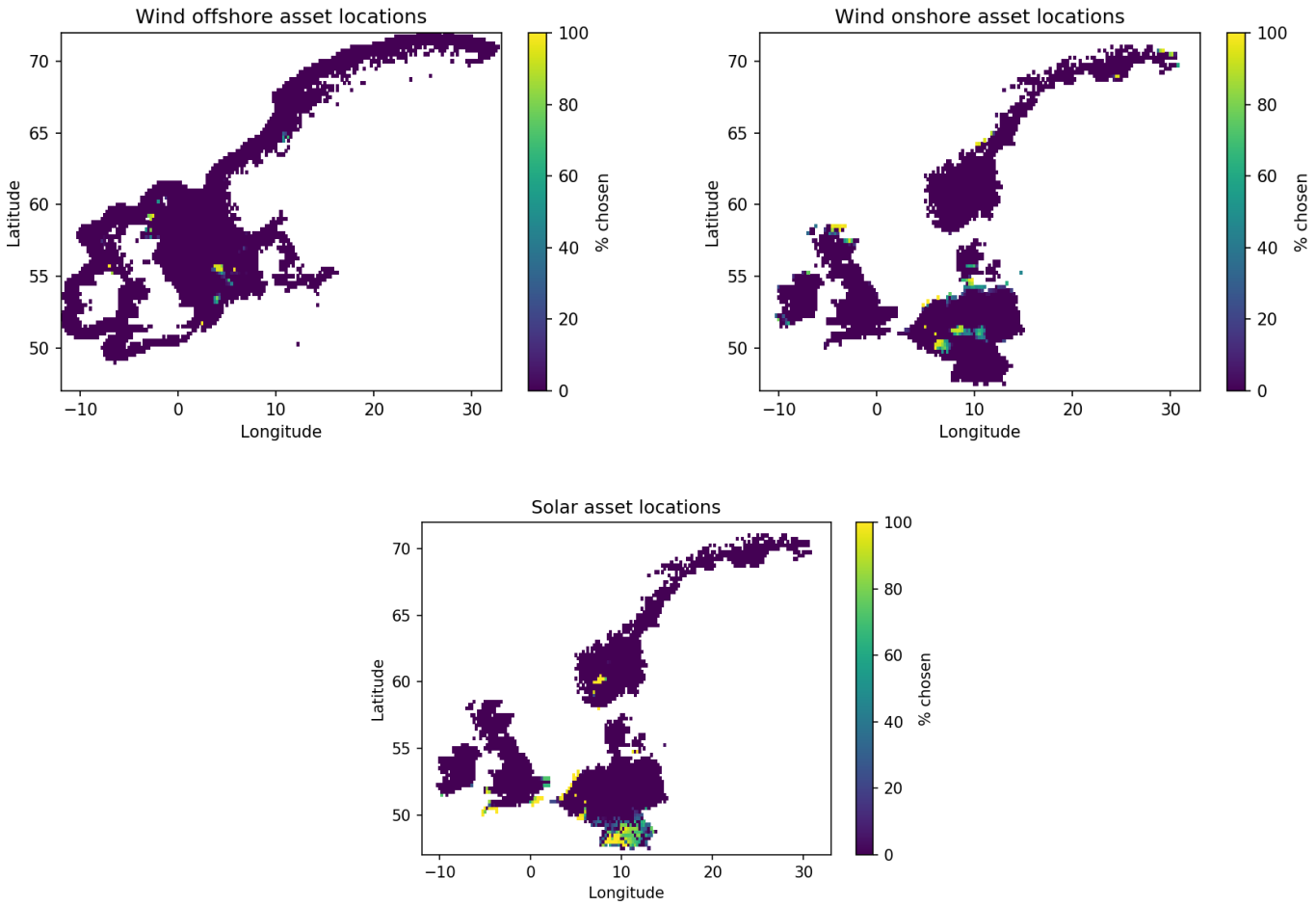

Figure 21: Percentage of locations chosen for portfolios on the efficient frontier, constrained scenario

3.5 Demand Response Scenarios

The DR scenario was explored to further investigate the role that DR can have to maximize the covariance of the constrained scenario. The efficient frontier for the DR scenario shows a similar trend as the other scenarios, see Figure 22. The Figure demonstrates that by employing DR the covariance can be positively influenced. The portfolio with the highest return when DR is applied has a 10% higher covariance for the max return portfolio compared to the normal constrained scenario. At the maximum covariance point this is 6.5 %.

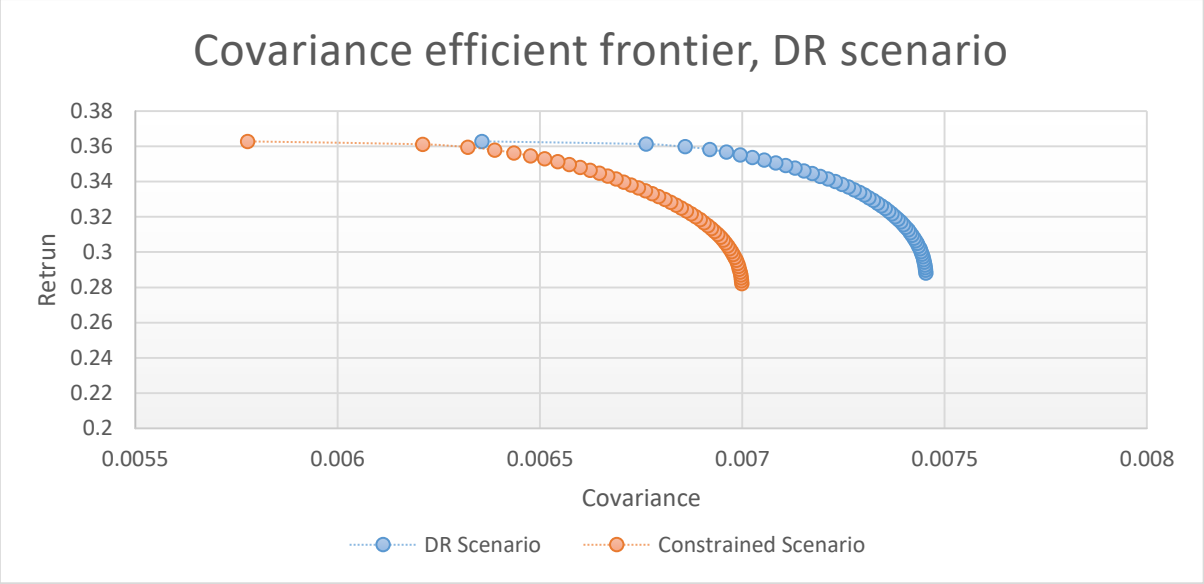

Figure 22: Covariance efficient frontier for DR and constrained scenario

A similar trend can be observed when looking at the correlation, see Figure 23. There is about a 2.7 % increase in correlation at maximum return portfolio while there is 2.4 % increase at the maximum covariance point. Adding DR under a 12-hour DR potential can lead to a maximum correlation of about 30 % between the electricity demand and VRE production. The somewhat lesser increase at the maximum covariance portfolio can be attributed to that DR is optimized for the electricity production at the portfolio with the maximum energy output and not the maximum covariance.

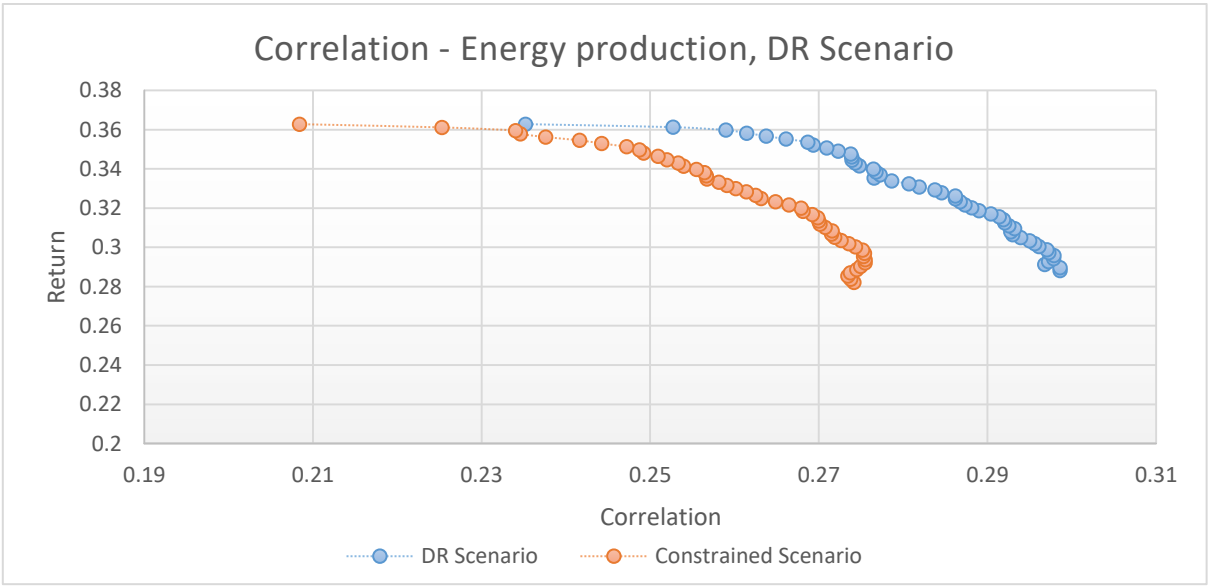

Figure 23: Correlation between Return and demand using demand response

3.5.1 Sensitivity Analysis DR

Iterating the DR optimization over changing DR duration as well as potential showed that the covariance is maximized when the DR duration (of 48 hours) is maximum as well, see Figure 24. Figure 24 shows that the variation between the covariance efficient frontiers of the DR runs is considerable. Furthermore, while the increasing the potential and duration generally increases the covariance of the max-return portfolio this is not true for the whole period.

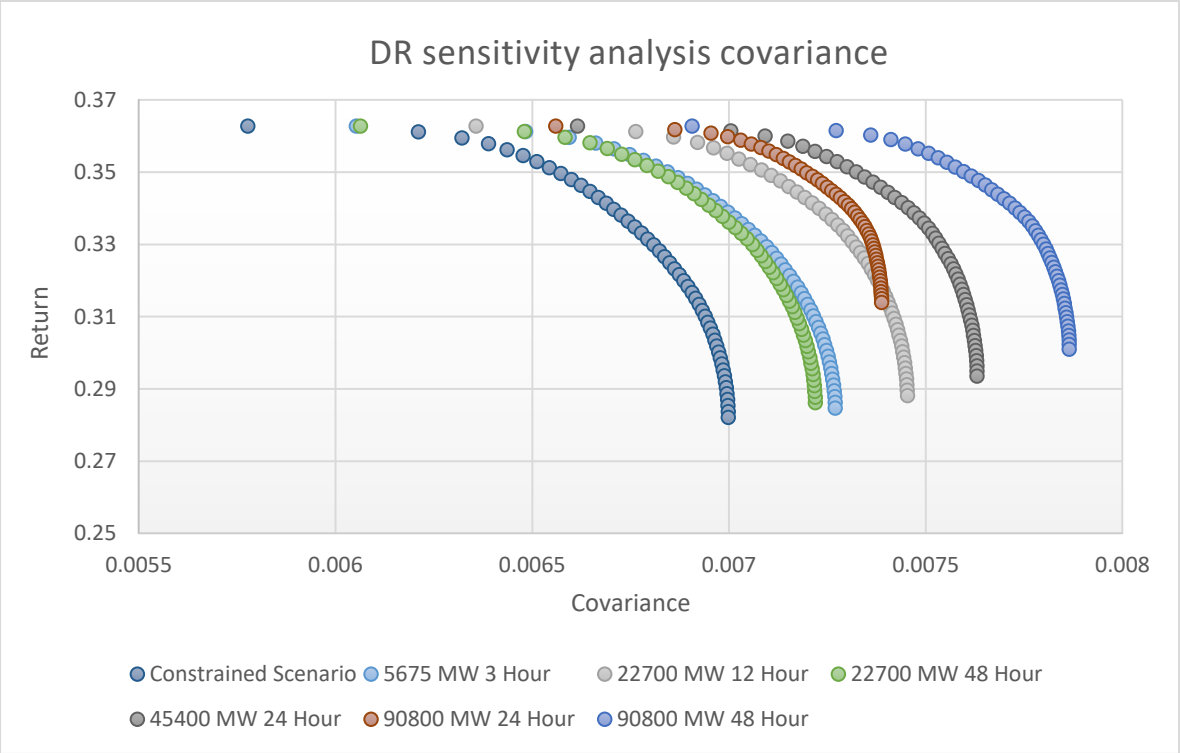

Figure 24: DR sensitivity analysis covariance, changing the magnitude (in MW) and duration (in hour)

Similar to the cases of constrained and unconstrained optimization, the DR portfolios with the maximum covariance are not the same as the DR portfolios with the maximum correlation. Figure 25, shows that the DR scenario that has the highest potential but a duration of 24 hours produces the largest correlation of 0.316. This further solidifies the view that maximizing the covariance might not necessarily mean that the correlation is also maximized. The DR scenario with a 48-hour time shift and with the highest covariance takes the second place in Figure 25.

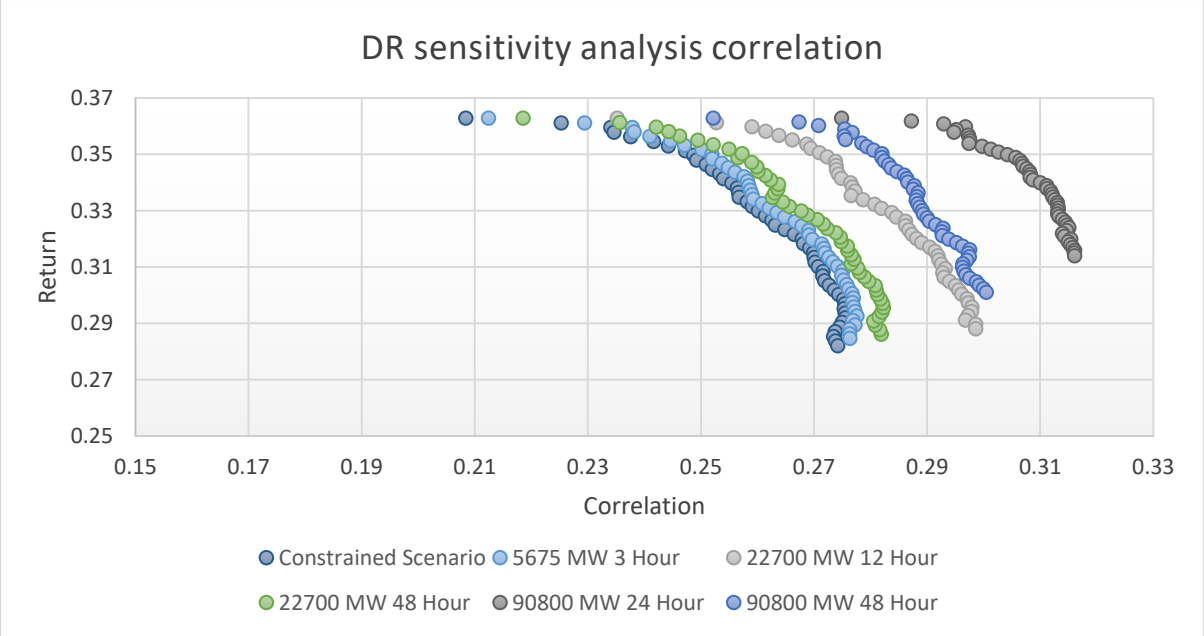

Figure 25: DR sensitivity analysis correlation

3.6 Scenario Comparison

Figure 12 and Figure 17 side-by-side show that the covariance of the unconstrained scenario is a lot higher compared to the constrained one. However, when comparing the correlation graphs, Figure 13 and Figure 18, it becomes clear that this relationship is not mirrored in the correlation between the portfolio and the energy demand, since the correlation of the constrained portfolio is higher than that of the unconstrained one. At first, this observation might seem counter-intuitive but the reason for this difference is that correlation is unit-less while the covariance is not. The unconstrained scenario is able to pick higher CF output locations compared to the constrained scenario. This results in both a higher return and higher covariance.

The correlation between production and demand is also dependent on their respective variances. Figure 26, shows the difference between the variance of the two scenarios. The variance of both scenarios decreases relatively more with when the return is lower. Additionally, the variance of the portfolios of the constrained scenario is lower than that of the unconstrained scenario. This difference explains why the correlation is higher for the constrained scenario (since computing the correlation requires dividing by smaller numbers). Maximizing the covariance is therefore biased towards the maximizing the return.

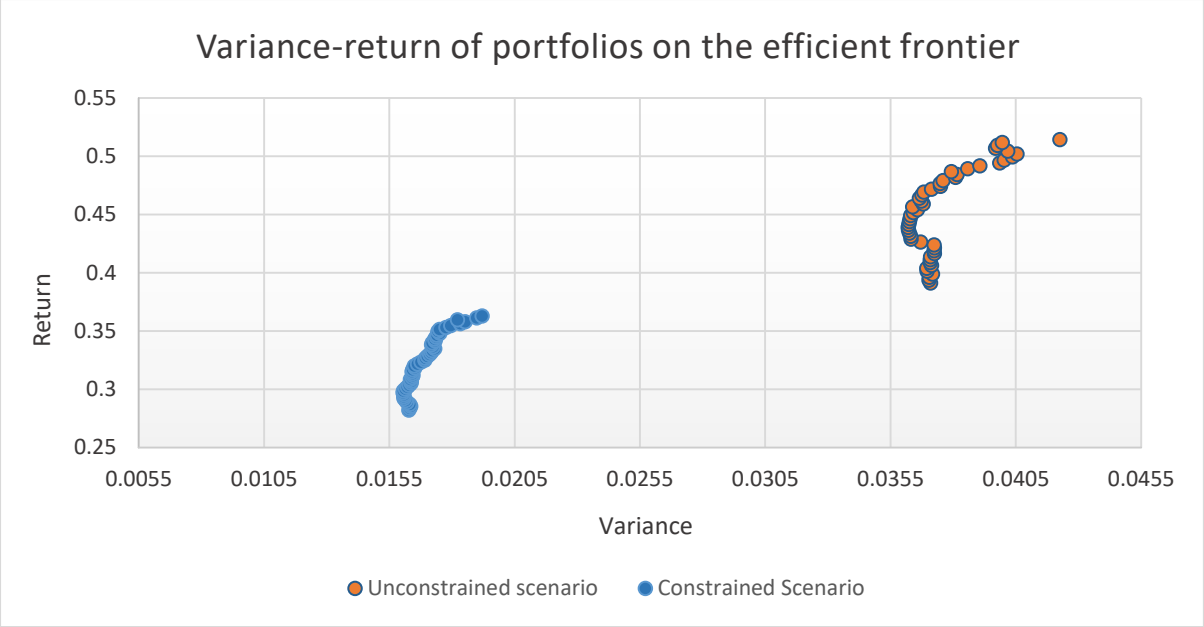

Figure 26: Variance-return graph of the unconstrained and constrained scenario

Not only is the correlation higher for the constrained scenario, there is also more variation in the power delivered, see Table 3-1. For the max return portfolio only 0.14% of the load is met at the point of lowest share of VRE production to demand and producing a surplus of 137 422 MW at the maximum over-production point. The constrained scenario is better able to meet the demand, however, at a minimum there is a considerable amount of demand unmet. DR helps in that sense as it especially reduces the over-production. The max return portfolios are able to meet more of the baseload demand but also have more variation in their output.

From the cumulative installed capacity presented in Table 3-1, it can be seen that wind offshore could be the cause of more over-production, when comparing the max-return versus the max covariance unconstrained portfolio. DR changes relatively little of the division between solar and wind, however, directing a little more installed capacity to wind onshore.

Table 3-1: Results of max return & max covariance portfolios of unconstrained and constrained optimization scenarios

Installed capacity (MW)	Max-return			Max-Covariance		
Scenario	**Unconstrained**	**Constrained**	**DR**	**Unconstrained**	**Constrained**	**DR**
Wind onshore	13 500	116 451	116 451	196 017	120 964	121 300
Wind offshore	263 845	72 008	72 008	81 278	67 495	67 120
Solar PV	0	88 835	88 835	0	88 835	88 835
% of demand met						
Max Over production (MW)	241% (137 422)	153.9% (74 730)	144.6% (49 752)	215% (125 931)	142.8% (55 622)	140.5% (43 461)
Min Under production (MW)	0.14% (-128 362)	4.4% (-103 638)	4.3% (-106 556)	0.44% (-168 802)	2.2% (-169 659)	2.8% (-139 469)
Standard deviation	46.7	25.3	24.8	43.5	22.0	22.2
Mean	90.2	60	59.7	71.6	48.0	49.4

The standard deviation (SD) and mean of the % of demand met for the various portfolios give more insight than just the amount of over and under production, also see Figure 27. The mean shows that while the over production and under production might be big, the mean power output is the highest for the unconstrained scenario. However, the standard deviation of this portfolio is also the highest. The lowest standard deviation is for the DR maximum covariance portfolio. Nevertheless, the mean in this scenario is the lowest. This shows that having a high mean also leads to a higher standard deviation.

The histograms in Figure 27 further confirms this story. The constrained covariance portfolio has the lowest mean but also the lowest SD of the four plotted portfolios. It also has the highest certainty of meeting demand, at around 40% of the demand. Furthermore, the somewhat irregular shape of the max-return unconstrained portfolio is smoothened out by the covariance optimization. Additional histograms of the DR scenario and the DR scenario with the highest correlation can be found in Appendix C: Scenario histograms .

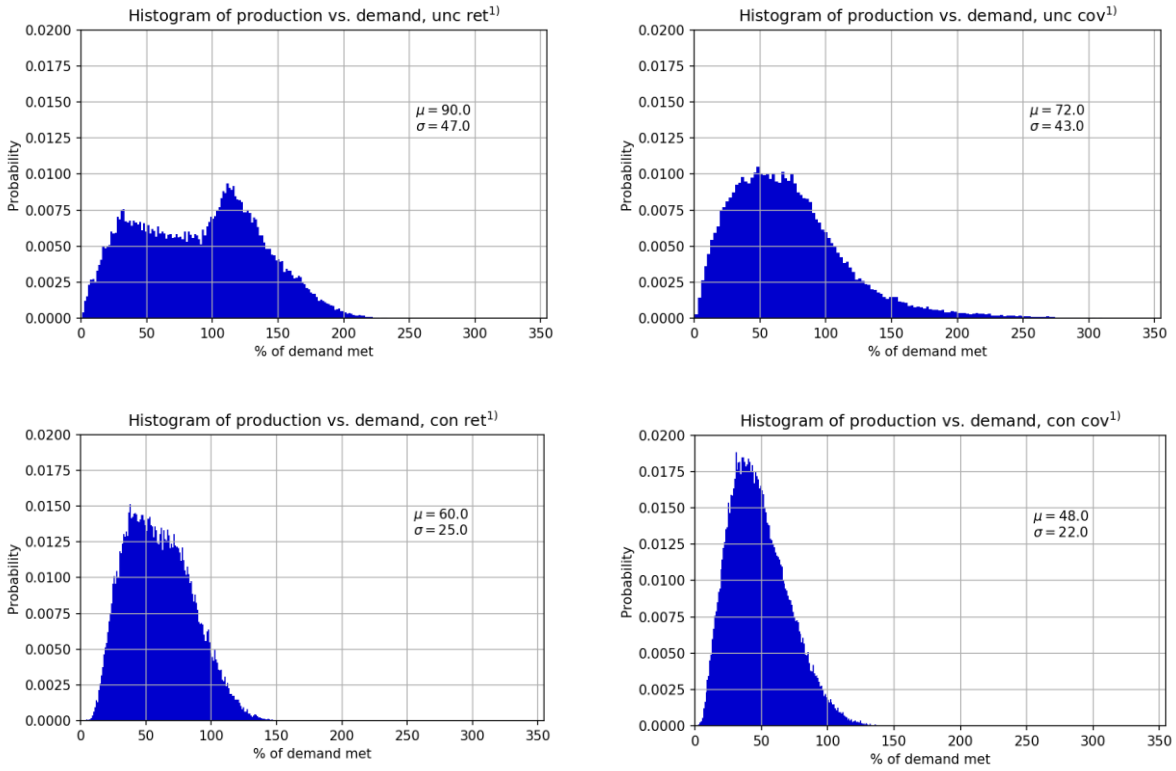

Figure 27: Histograms percentage of demand met of four portfolios for 9 years of data. [1)]Refers to the scenarios and portfolios respectively: unc stands for unconstrained, con for constrained, ret for max-return portfolio and cov for max-covariance portfolio.

4. Discussion

This thesis set out to investigate to what extent the covariance between energy production and demand can be maximized. The results indicate that the locations of VRE assets have a significant role in varying this extent. The constrained scenario further confirmed this but also showed that the portfolio with the highest correlation and covariance do not necessarily align, as the correlation for the constrained scenario is higher than that of the unconstrained one. The discussion is structured as follows; first, this study's results are compared with other literature. Second, the limitations and future research are discussed.

4.1 Comparison to other work

4.1.1 Comparison to other literature

The principal difference between the constrained and the unconstrained scenario is that when solar power is included, the overall correlation with the energy demand increases. This is in line with previous research, which states that geographically dispersed solar PV can increase the correlation between electricity production and demand [113]. Furthermore, the variance of the portfolio's output is also decreased due to solar PV uptake, which is in line with [13,14], as they found that including solar in one's portfolio decreases the portfolio's variance but not the portfolio's output. It is therefore beneficial to include solar PV in the portfolios but this will have an effect on the portfolio's output.

The optimization performed by this study was the first of its kind. It was therefore difficult to compare the locations chosen as well as the overall output used by this study with other studies as also the region and expected installed capacity differed. However, it was possible to compare the results of the locations to some extent. The asset locations of the constrained maximum covariance portfolio match closely to [114], especially for solar PV and wind onshore. The optimization of that study [114], aimed to minimize the standard deviation of wind and solar but using locations based on 2020 targets. The locations found by this study are different than that of [16,19]. Possibly this is due to the reduced area studied in this thesis as well as a difference in the optimization problem formulation.

The results found by [23] in their portfolio analysis for the European Union, showed that demand can be met 6.38% with a 97.7% probability when assuming a wind total installed capacity of 240 GW. In comparison the results of this thesis showed that all portfolios exhibit a probability of 100% or 99.4% meeting 6.38% of the demand, providing superior results. The portfolios on the efficient frontiers have at least a 97.8% probability of meeting 11% of the demand. The contrast can potentially be explained by the difference in installed capacity and region chosen as [23] does not include Norway and the North Sea in their analysis. Furthermore, [23] only uses 2008 demand making actual comparison not clear cut.

4.1.2 Comparison to already installed capacity

The findings showed that particular locations are to be preferred to increase either overall power output, covariance or points in between. This optimization however, did not include already installed capacities. Figure 28 shows the already installed offshore locations from [93] with the model output locations of the constrained and unconstrained scenario. This shows that there is little overlap between the locations chosen by the model and the locations that are already built in real life. This means that the locations are neither optimal for optimizing the return of the whole region or the covariance with the demand.

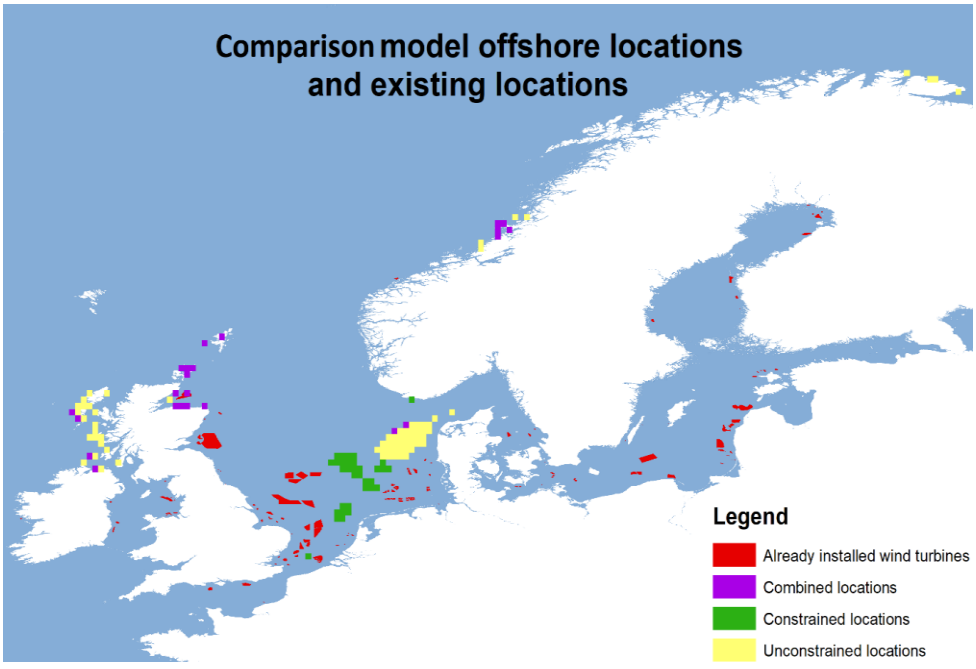

Figure 28: Model wind offshore locations versus already installed wind turbines. Map produced by author based on sea outline [93,115]

4.2 Limitations & Future Research

The constrained optimization showed that while the covariance is lower compared to the unconstrained scenario the correlation is not. Also, the standard deviation of the constrained scenarios was much lower. It might therefore be better to perform a mean correlation optimization. In that way the demand pattern is more exactly followed. However, this does mean that a lower overall electricity production needs to be accepted. In maximizing the correlation, DR could provide a valuable addition as it increases the percentage of demand met while also decreasing the standard deviation of this.

Various factors that influence the output of solar panels and wind turbines were not taken into account. For example, including a factor to account for the shadow of buildings and other objects would have provided more accurate results. Additionally, it was assumed that solar PV could not be installed offshore and that solar PV could be installed together with onshore turbines without a decrease of solar PV efficiency due to shadowing.

It would beneficial to conduct the analysis for a wider range of chosen technologies to further fine tune the results. For example, picking 10 different turbines and 10 different solar panels and or varying the physical constraints, such as tilt angle and hub height. This would allow for more robust results.

The case study area was large enough to show a clear difference between optimizing for return and optimizing for covariance. However, a larger area could have led to an increase in covariance. Due to computation time constraints, this was not deemed feasible but future research could benefit by including additional area in their study.

The weather model and thus the weather data used in this thesis was used without correction factor[1]. Research has shown that by applying a correction factor to weather models, such as MERRA and MERRA-2, it will lead to an increase in accuracy [116,117]. While ERA5 is more accurate than MERRA-2, it still is not perfectly correlated with local data [37]. However, correction factors were not available at the time of research and was thus not used.

[1] A correction factor scales the weather date such that is more accurately represents local weather data.

It was assumed that all the VRE assets could be installed in the most optimal spots. However, since the timeframe of study is 2030, already installed assets might be still in place as the typical age of wind turbines is 20 years [118], and at least 25 years for solar PV [63]. Additional research could look into these locations and set them as constraints in the optimization such that these locations have to be picked. Existing transmission infrastructure was also not taken into account. While being somewhat approximated with the constrained scenario, adding them would portray a more accurate representation of reality.

The usable area computed in this study is an assumption that heavily influences the outcomes of the analysis. The constraints were computed using bilinear interpolation, which is in essence an additional assumption. Future research could instead calculate the percentage of area of each suitability factor in each grid cell and combine that together with the weights to form one suitability value per grid cell.

The portfolios that lie on the efficient frontier showed that over- and underproduction occurred. From a system analysis point of view, it would be beneficial for future research to include other technologies to investigate what additional technologies would be needed so that the demand could be better met. This would also show different optimal mixes of technologies when analysing the portfolios that lie on the efficient frontier. Additionally, the total levelized cost of electricity of such a system could be included making further selection of the optimal VRE portfolio potentially easier and more financially intuitive.

The DR applied in this study assumed perfect foresight, activation times that are possible within the hour and duration uniformity across the duration of DR as well as unlimited dispatch potential per annum. However, this is not always the case in reality [11]. Furthermore, the potentials used in this study rest on the technical potential meaning that the actual usable potential might be lower. Nevertheless, the lowest technical DR potential in [11] was used in this thesis. The real contribution of DR to increase the covariance might therefore be lower. Due to the unique objective function as well as due to applying DR to an aggregated region that is somewhat unique made comparison with other literature on the changed demand profile difficult.

The DR optimization was aimed at maximizing the max return portfolio for the constrained scenario. However, future research could look into co-optimizing the covariance and DR such that

maximum covariance portfolio is optimized for Demand Response. This would change the objective function and the optimization problem. Due to time constraints this was not done in this thesis.

A Mean Variance Analysis (MVA) could be computed together with the MCVA. This would show the trade-offs between minimizing for variance and maximizing for covariance. Such results could indicate where the trade-offs are and what percentage of demand can be met with an MVA.

Lastly, the weather data used in this study was historic and assumed to be a representative set of all-weather variation. The duration of the weather data was however limited as the historic demand data for the region was limited to 9 years. Using more of the available weather data would have made the production part of the analysis more robust but it would also mean that additional demand patterns needed to be created. Since estimating demand patterns from weather patterns and other historic demand data was outside of the scope of this research, 9 years of weather data was used. Additionally, due to climate change, both electricity production and demand will change in the future [119,120]. However, since it is difficult to determine to what extent the climate will change [121] by 2030 as well as only having 12 years between the data and 2030 climate change influences were not used in this study.

4.3 Implications

The results of this thesis showed that when installing VRE technologies in locations that are solely used for maximizing electricity output a high variation in electricity output occurs. It would therefore be beneficial to create some sort of subsidy for electricity producers to install VRE assets in one region instead of the other. This thesis's findings of dispersing VRE location, rather implicitly, aligns with existing studies and plans [16,23] to further improve transmission capabilities in Europe as such a network can benefit the integration of VRE technologies in the energy system.

The results further indicate that the model prefers wind onshore installation with respect to wind offshore. This is in line what is currently being done in Europe, as the share of installed onshore capacity is higher than that of offshore wind [73].

Furthermore, while maximizing the covariance in the unconstrained scenario it still means that there is a relative large standard deviation of the ratio between the demand and production compared to the constrained scenarios. The portfolios selected in the constrained scenario might therefore be preferred by grid operators or policy makers since there is less variability in their output. A MCVA might therefore not be the most ideal optimization to select the locations of VRE technologies. A MVA or mean correlation analysis (with a minimum ratio constrained) might in this sense be a better fit.

5. Conclusion

This thesis used portfolio theory to investigate to what extent the covariance between VRE production and demand can be maximized and what effect it would have on the placement and installed capacity of VRE assets such as solar and wind farms. Demand response was also explored as an addition to strategically place VRE production to maximize the covariance. Herein, 9 years of demand and weather data for the Northwest Europe was used as a basis for the analysis.

The results showed that by changing the locations and capacity of VRE assets in Northwest Europe, the covariance between VRE production and electricity demand can be maximized, depending on the imposed restrictions. DR can further increase this covariance. The locations of these VRE assets were distributed across the studied region. For maximum covariance or maximum return, the unconstrained optimization only selected wind onshore and offshore locations. When the scenario was constrained to reflect national RES targets this distribution changed and solar PV was integrated. This resulted in a lower overall electricity production but also more correlation with the electricity demand. The correlation and covariance were further increased by implementing DR.

The ratio of production and demand of the different scenarios also showed that it might be preferred to pick portfolios with a higher correlation as they are able to meet demand in a more consistent way. DR can perform an active role in this optimization as the covariance and correlation can both be increased. However, optimizing for correlation comes at a cost of a decrease in VRE output.

The locations and usage of VRE assets mostly differs across all optimizations. If possible, it is therefore recommended to investigate the possible locations of large-scale VRE installations before building occurs as this can greatly influence the extent other resources are needed to either fill the gap to meet demand or to balance the electricity grid. If more variation can be accepted, a high return or high covariance portfolio can be accepted. If smaller variation in the ratio between production and demand is desired, a constrained scenario might be preferred.

To conclude, covariance optimization leads to portfolios of VRE assets that follow the demand to some extent while still having relatively high VRE output. Portfolios where the correlation is higher

show that a further lowering of the output needs to be accepted in return for a better match with the demand. Demand response has a positive effect on both the covariance and correlation and could be a good addition to location-optimized VRE production.

6. Acknowledgements

I would like to thank the academic staff at the Copernicus Institute for providing me with the background needed to complete this study. Especially the feedback and insightful questions of Prof. dr. Madeleine Gibescu were greatly appreciated as it improved the quality of my research as well as this thesis. I would also like to thank Jing Hu, MSc. for his input and answers to my numerous questions on portfolio theory, R studio and Mean (Co)Variance optimization, it greatly improved my understanding of these concepts and made it possible to integrate them easier. I would also like to thank Laurens Stoop, MSc. for his time and help with netcdf files and their analysis in Python. The Python data analysis would not have been able run so smoothly without him. Lastly, I would like to thank my girlfriend Sara Hogye, MSc for her support, input and discussions. My thesis would not look like as it does now without her.

7. Bibliography

[1] Pixabay, agriculture alternative energy clouds countryside, (n.d.). https://www.pexels.com/photo/agriculture-alternative-energy-clouds-countryside-414837/ (accessed August 14, 2019).

[2] P. Nørgaard, H. Holttinen, A Multi-Turbine Power Curve Approach, Nord. Wind Power Conf. (2004) 5.

[3] R. Lacal Arantegui, A. Jäger-Waldau, Photovoltaics and wind status in the European Union after the Paris Agreement, Renew. Sustain. Energy Rev. 81 (2018) 2460–2471. doi:10.1016/j.rser.2017.06.052.

[4] European Commission, 2030 climate & energy framework, (n.d.). https://ec.europa.eu/clima/policies/strategies/2030_en (accessed July 30, 2019).

[5] H.W. Sinn, Buffering volatility: A study on the limits of Germany's energy revolution, Eur. Econ. Rev. 99 (2017) 130–150. doi:10.1016/j.euroecorev.2017.05.007.

[6] R.A. Verzijlbergh, L.J. De Vries, G.P.J. Dijkema, P.M. Herder, Institutional challenges caused by the integration of renewable energy sources in the European electricity sector, Renew. Sustain. Energy Rev. 75 (2017) 660–667. doi:10.1016/j.rser.2016.11.039.

[7] H. Shaker, H. Zareipour, D. Wood, Impacts of large-scale wind and solar power integration on California's net electrical load, Renew. Sustain. Energy Rev. 58 (2016) 761–774. doi:10.1016/j.rser.2015.12.287.

[8] T.A. Deetjen, J.D. Rhodes, M.E. Webber, The impacts of wind and solar on grid flexibility requirements in the Electric Reliability Council of Texas, Energy. 123 (2017) 637–654. doi:10.1016/j.energy.2017.02.021.

[9] P.D. Lund, J. Lindgren, J. Mikkola, J. Salpakari, Review of energy system flexibility measures to enable high levels of variable renewable electricity, Renew. Sustain. Energy Rev. 45 (2015) 785–807. doi:10.1016/j.rser.2015.01.057.

[10] L. Söder, P.D. Lund, H. Koduvere, T.F. Bolkesjø, G.H. Rossebø, E. Rosenlund-Soysal, K. Skytte, J. Katz, D. Blumberga, A review of demand side flexibility potential in Northern Europe, Renew. Sustain. Energy Rev. 91 (2018) 654–664. doi:10.1016/j.rser.2018.03.104.

[11] H.C. Gils, Assessment of the theoretical demand response potential in Europe, 67 (2014). doi:10.1016/j.energy.2014.02.019.

[12] B. Drake, K. Hubacek, What to expect from a greater geographic dispersion of wind farms?-A risk portfolio approach, Energy Policy. 35 (2007) 3999–4008. doi:10.1016/j.enpol.2007.01.026.

[13] M. Shahriari, S. Blumsack, The capacity value of optimal wind and solar portfolios, Energy. 148 (2018) 992–1005. doi:10.1016/j.energy.2017.12.121.

[14] J. Hu, R. Harmsen, W. Crijns-Graus, E. Worrell, Geographical optimization of variable renewable energy capacity in China using modern portfolio theory, Appl. Energy. 253 (2019) 113614. doi:10.1016/j.apenergy.2019.113614.

[15] F. Roques, C. Hiroux, M. Saguan, Optimal wind power deployment in Europe e a portfolio approach., Robert Schuman Cent. Adv. Stud. (2009). doi:10.2139/ssrn.2481918.

[16] W. Zappa, M. van den Broek, Analysing the potential of integrating wind and solar power in Europe using spatial optimisation under various scenarios, Renew. Sustain. Energy Rev. 94 (2018) 1192–1216. doi:10.1016/j.rser.2018.05.071.

[17] F. Cassola, M. Burlando, M. Antonelli, C.F. Ratto, Optimization of the regional spatial distribution of wind power plants to minimize the variability of wind energy input into power supply systems, J. Appl. Meteorol. Climatol. 47 (2008) 3099–3116. doi:10.1175/2008JAMC1886.1.

[18] W.D. Grossmann, I. Grossmann, K.W. Steininger, Distributed solar electricity generation across large geographic areas, Part I: A method to optimize site selection, generation and storage, Renew. Sustain. Energy Rev. 25 (2013) 831–843. doi:10.1016/j.rser.2012.08.018.

[19] T. Van der Vliet, The effect of storage and interconnection on the optimal mix of intermittent renewables in Europe, (2015).

[20] Y. Rombauts, E. Delarue, W. D'haeseleer, Optimal portfolio-theory-based allocation of wind power: Taking into account cross-border transmission-capacity constraints, Renew. Energy. 36 (2011) 2374–2387. doi:10.1016/j.renene.2011.02.010.

[21] F. DeLlano-Paz, A. Calvo-Silvosa, S.I. Antelo, I. Soares, Energy planning and modern

portfolio theory: A review, Renew. Sustain. Energy Rev. 77 (2017) 636–651. doi:10.1016/j.rser.2017.04.045.

[22] F. Cucchiella, I. D'Adamo, M. Gastaldi, Optimizing plant size in the planning of renewable energy portfolios, Lett. Spat. Resour. Sci. 9 (2016) 169–187. doi:10.1007/s12076-015-0150-6.

[23] C. Tejeda, C. Gallardo, M. Domínguez, M.Á. Gaertner, C. Gutierrez, M. de Castro, Using wind velocity estimated from a reanalysis to minimize the variability of aggregated wind farm production over Europe, Wind Energy. 21 (2018) 174–183. doi:10.1002/we.2153.

[24] H. Markowitz, Portfolio Selection, J. Finance. 7 (1952) 77–91.

[25] J.C. Francis, D. Kim, Modern Portfolio Theory: Foundations, Analysis, and New Developments, Wiley, 2013.

[26] ENTSOE, Monthly Hourly Load Values, (2019). https://www.entsoe.eu/data/power-stats/hourly_load/.

[27] T. Müller, D. Möst, Demand Response Potential: Available when Needed?, Energy Policy. 115 (2018) 181–198. doi:10.1016/j.enpol.2017.12.025.

[28] RESPOND, Demand-Side Management vs. Demand Response, (n.d.). http://project-respond.eu/demand-side-management-vs-demand-response/ (accessed July 31, 2019).

[29] M. Qadrdan, M. Cheng, J. Wu, N. Jenkins, Benefits of demand-side response in combined gas and electricity networks, Appl. Energy. 192 (2017) 360–369. doi:10.1016/j.apenergy.2016.10.047.

[30] N. O'connell, P. Pinson, H. Madsen, M. Omalley, Benefits and challenges of electrical demand response: A critical review, Renew. Sustain. Energy Rev. 39 (2014) 686–699. doi:10.1016/j.rser.2014.07.098.

[31] A. Kies, B.U. Schyska, L. Von Bremen, The Demand Side Management Potential to Balance a Highly Renewable European Power System, (2016) 1–14. doi:10.3390/en9110955.

[32] EEA, Europe's onshore and offshore wind energy potential, Copenhagen, 2009. doi:10.2800/11373.

[33] Flanders Marine Institute, Union of the ESRI Country shapefile and the Exclusive

Economic Zones (version 2), (2014). http://www.marineregions.org/.

[34] Eurostat, Countries 2016, (2019). https://ec.europa.eu/eurostat/web/gisco/geodata/reference-data/administrative-units-statistical-units/countries.

[35] GEBCO compilation group, GEBCO 2019 Grid, (2019). doi:doi:10.5285/836f016a-33be-6ddc-e053-6c86abc0788e.

[36] T. Huld, R. Urraca, A.G. Amillo, J. Trentmann, A Global Hourly Solar Radiation Data set Using Satellite and Reanalysis Data, 33rd Eur. Photovolt. Sol. Energy Conf. Exhib. (2017) 2458–2462.

[37] J. Olauson, ERA5: The new champion of wind power modelling?, Renew. Energy. 126 (2018) 322–331. doi:10.1016/j.renene.2018.03.056.

[38] H. Hersbach, L. Dick, ERA5 reanalysis is in production, ECMWF Newsl. (2016). http://www.ecmwf.int/sites/default/files/elibrary/2016/16299-newsletter-no147-spring-2016.pdf.

[39] Copernicus Climate Service, Climate reanalysis, (n.d.). https://climate.copernicus.eu/climate-reanalysis (accessed April 10, 2019).

[40] R.J. Davy, A. Troccoli, Interannual variability of solar energy generation in Australia, Sol. Energy. 86 (2012) 3554–3560. doi:10.1016/j.solener.2011.12.004.

[41] S. Jerez, F. Thais, I. Tobin, M. Wild, A. Colette, P. Yiou, R. Vautard, The CLIMIX model: A tool to create and evaluate spatially-resolved scenarios of photovoltaic and wind power development, Renew. Sustain. Energy Rev. 42 (2015) 1–15. doi:10.1016/j.rser.2014.09.041.

[42] W. F. Holmgren, C. W. Hansen, M. A. Mikofski, Pvlib Python: a Python Package for Modeling Solar Energy Systems, J. Open Source Softw. 3 (2018) 884. doi:10.21105/joss.00884.

[43] J. Twidell, T. Weir, Renewable Energy Resources, Third, Routledge, 2015.

[44] G.B.M.A. Litjens, E. Worrell, W.G.J.H.M. van Sark, Influence of demand patterns on the optimal orientation of photovoltaic systems, Sol. Energy. 155 (2017) 1002–1014. doi:10.1016/j.solener.2017.07.006.

[45] J.A. Reindl, D.T.; Beckman, W.A.; Duffie, Diffuse Fraction Correlations. Sol. Energy,

45, (1990) 1–7.

[46] A. Dobos, PVWatts Version 5 Manual, (2014). doi:10.2172/1158421.

[47] R. Urraca, T. Huld, A. Gracia-Amillo, F.J. Martinez-de-Pison, F. Kaspar, A. Sanz-Garcia, Evaluation of global horizontal irradiance estimates from ERA5 and COSMO-REA6 reanalyses using ground and satellite-based data, Sol. Energy. 164 (2018) 339–354. doi:10.1016/j.solener.2018.02.059.

[48] R. Hogan, Radiation Quantities in the ECMWF model and MARS, 2015.

[49] J. Xie, M. Sengupta, Performance Analysis of Transposition Models Simulating Solar Radiation on Inclined Surfaces, Eur. PV Sol. Conf. Exhib. (EU PVSEC). 18302 (2016).

[50] K.N. Shukla, S. Rangnekar, K. Sudhakar, Comparative study of isotropic and anisotropic sky models to estimate solar radiation incident on tilted surface: A case study for Bhopal, India, Energy Reports. 1 (2015) 96–103. doi:10.1016/j.egyr.2015.03.003.

[51] J.A. Duffie, W.A. Beckman, Solar Engineering of Thermal Processes, Fourth, Wiley, Hoboken, 2013.

[52] J.D. Mondol, Y.G. Yohanis, B. Norton, Solar radiation modelling for the simulation of photovoltaic systems, Renew. Energy. 33 (2008) 1109–1120. doi:10.1016/j.renene.2007.06.005.

[53] A.M. Noorian, I. Moradi, G.A. Kamali, Evaluation of 12 models to estimate hourly diffuse irradiation on inclined surfaces, Renew. Energy. 33 (2008) 1406–1412. doi:10.1016/j.renene.2007.06.027.

[54] S. Dervishi, A. Mahdavri, A Comparison of Luminous efficacy models for the diffuse component of Solar radiation, Fourth Ger. IBPSA Conf. (2012) 117–120.

[55] Z. Li, H. Xing, S. Zeng, J. Zhao, T. Wang, Comparison of Anisotropic Diffuse Sky Radiance Models for Irradiance Estimation on Building Facades, Procedia Eng. 205 (2017) 779–786. doi:10.1016/j.proeng.2017.10.010.

[56] P. Yadav, S.S. Chandel, Comparative analysis of diffused solar radiation models for optimum tilt angle determination for Indian locations, Appl. Sol. Energy. 50 (2014) 53–59. doi:10.3103/s0003701x14010137.

[57] E.D. Mehleri, P.L. Zervas, H. Sarimveis, J.A. Palyvos, N.C. Markatos, Determination of the optimal tilt angle and orientation for solar photovoltaic arrays, Renew. Energy. 35

(2010) 2468–2475. doi:10.1016/j.renene.2010.03.006.

[58] D.T. Reindl, W.A. Beckman, J.A. Duffie, Evaluation of hourly tilted surface radiation models, Sol. Energy. 45 (1990) 9–17. doi:10.1016/0038-092X(90)90061-G.

[59] P.G. Loutzenhiser, H. Manz, C. Felsmann, P.A. Strachan, T. Frank, G.M. Maxwell, Empirical validation of models to compute solar irradiance on inclined surfaces for building energy simulation, Sol. Energy. 81 (2007) 254–267. doi:10.1016/j.solener.2006.03.009.

[60] Ecotality, What Are the Most Efficient Solar Panels of 2019?, (2019). https://ecotality.com/most-efficient-solar-panels/ (accessed April 25, 2019).

[61] SunPower, SunPower X-Series:X22-370, (2019).

[62] T. Hoium, Why Efficiency Doesn't Rule In Utility Solar, (2016). https://www.fool.com/investing/2016/10/19/why-efficiency-doesnt-rule-in-utility-solar.aspx (accessed April 25, 2019).

[63] TrinaSolar, Tallmax module, TSM-PD14, (2017).

[64] T. Doyle, T. Erion-Lorico, R. Deshamais, 2018 PV MODULE RELIABILITY SCORECARD, 2018.

[65] M.Z. Jacobson, V. Jadhav, World estimates of PV optimal tilt angles and ratios of sunlight incident upon tilted and tracked PV panels relative to horizontal panels, Sol. Energy. 169 (2018) 55–66. doi:10.1016/j.solener.2018.04.030.

[66] M. Šúri, T.A. Huld, E.D. Dunlop, H.A. Ossenbrink, Potential of solar electricity generation in the European Union member states and candidate countries, Sol. Energy. 81 (2007) 1295–1305. doi:10.1016/j.solener.2006.12.007.

[67] M. Hartner, A. Ortner, A. Hiesl, R. Haas, East to west - The optimal tilt angle and orientation of photovoltaic panels from an electricity system perspective, Appl. Energy. 160 (2015) 94–107. doi:10.1016/j.apenergy.2015.08.097.

[68] S. Kichou, S. Silvestre, L. Guglielminotti, L. Mora-López, E. Muñoz-Cerón, Comparison of two PV array models for the simulation of PV systems using five different algorithms for the parameters identification, Renew. Energy. 99 (2016) 270–279. doi:https://doi.org/10.1016/j.renene.2016.07.002.

[69] Christopher P. Cameron, William E. Boyson, Daniel M. Riley, Comparison of PV

System Performance-Model Predictions with Measured PV System Performance, Conf. Rec. IEEE Photovolt. Spec. Conf. (2008) 2–7. doi:10.1109/PVSC.2008.4922865.

[70] N.J. Blair, A.P. Dobos, P. Gilman, Comparison of Photovoltaic Models in the System Advisor Model, 2013.

[71] S. Pfenninger, I. Staffell, Long-term patterns of European PV output using 30 years of validated hourly reanalysis and satellite data, Energy. 114 (2016) 1251–1265. doi:10.1016/j.energy.2016.08.060.

[72] D.L. King, W.E. Boyson, J.A. Kratochvil, Photovoltaic array performance model., Sandia National Laboratories, 2004. doi:10.2172/919131.

[73] WindEurope, Wind energy in Europe in 2018, (2018). https://windeurope.org/wp-content/uploads/files/about-wind/statistics/WindEurope-Annual-Statistics-2018.pdf.

[74] T. Telsnig, C. Vazquez Hernandez, A. Villalba Pradas, JRC Wind Energy Status Report, Jt. Res. Cent. (2017). doi:10.2760/332535.

[75] J. Manwell, J. McGowan, A. Rogers, Wind Energy Explained, Second, Wiley, 2009.

[76] M. Brower, B.H. Bailey, Wind resource assessment : a practical guide to developing a wind project, Wiley, 2012.

[77] J. Holmes, Wind Loading of Structures, Spon Press, 2010. doi:10.4324/9780203301647.

[78] I. Troen, E. Lundtang Petersen, European Wind Atlas, 1989. www.windatlas.dk/AuxiliaryFiles/images/EWA+web.jpg.

[79] International Electrotechincal Comission, IECC 61400-1, Edition 3.1, 2014.

[80] Wind-turbine-models, Vestas V112-3.45, (2016). https://en.wind-turbine-models.com/turbines/1247-vestas-v112-3.45 (accessed June 1, 2019).

[81] Wind-turbine-models, Vestas V126-3.45, (2016). https://en.wind-turbine-models.com/turbines/1249-vestas-v126-3.45 (accessed June 1, 2019).

[82] Wind-turbine-models, Vestas V136-3.45, (2015). https://en.wind-turbine-models.com/turbines/1282-vestas-v136-3.45 (accessed June 3, 2019).

[83] Thewindpower, V164/9500, (2019). https://www.thewindpower.net/turbine_en_1476_mhi-vestas-offshore_v164-9500.php.

[84] P.A. Lynn, Onshore and Offshore Wind Energy : An Introduction, John Wiley & Sons, Incorporated, Hoboken, UNITED KINGDOM, 2011.

http://ebookcentral.proquest.com/lib/uunl/detail.action?docID=819176.

[85] E. Son, S. Lee, B. Hwang, S. Lee, Characteristics of turbine spacing in a wind farm using an optimal design process, Renew. Energy. 65 (2014) 245–249. doi:10.1016/j.renene.2013.09.022.

[86] D. Pollak, Characterization of Ambient Offshore Turbulence Intensity from Analysis of Nine Offshore Meteorological Masts in Northern Europe, (2014).

[87] S. Haas, B. Schachler, U. Krien, S. Bosch, windpowerlib: A python library to model wind power plants (v0.1.1), (2019). https://windpowerlib.readthedocs.io/en/stable/getting_started.html#citing-the-windpowerlib.

[88] A. Colmenar-Santos, S. Campíñez-Romero, L.A. Enríquez-Garcia, C. Pérez-Molina, Simplified analysis of the electric power losses for on-shore wind farms considering weibull distribution parameters, Energies. 7 (2014) 6856–6885. doi:10.3390/en7116856.

[89] K. Eurek, P. Sullivan, M. Gleason, D. Hettinger, D. Heimiller, A. Lopez, An improved global wind resource estimate for integrated assessment models, Energy Econ. 64 (2017) 552–567. doi:10.1016/j.eneco.2016.11.015.

[90] J. Novacheck, J.X. Johnson, Diversifying wind power in real power systems, Renew. Energy. 106 (2017) 177–185. doi:10.1016/j.renene.2016.12.100.

[91] M.M. Hoogwijk, on the Global and Regional Potential of Renewable Energy, Utrecht, 2004.

[92] ESRI, Resample, (n.d.). https://pro.arcgis.com/en/pro-app/tool-reference/data-management/resample.htm (accessed June 15, 2019).

[93] EMODnet, Emodnet_HA_Wind_Farms_20180115, (2018). https://www.emodnet-humanactivities.eu/search-results.php?dataname=Wind+Farms+%28Polygons%29.

[94] EEA, Nationally designated aread (CDDA), (2019). https://www.eea.europa.eu/data-and-maps/data/natura-10#tab-gis-data.

[95] EEA, Natura 2000 data - the European network of protected sites, (2018). https://www.eea.europa.eu/data-and-maps/data/natura-9#tab-derived-datasets.

[96] CORINE Land Cover, CLC 2018, (2019). https://land.copernicus.eu/pan-european/corine-land-cover/clc2018?tab=download.

[97] Y.Y. Deng, M. Haigh, W. Pouwels, L. Ramaekers, R. Brandsma, S. Schimschar, J. Grözinger, D. de Jager, Quantifying a realistic, worldwide wind and solar electricity supply, Glob. Environ. Chang. 31 (2015) 239–252. doi:10.1016/j.gloenvcha.2015.01.005.

[98] J.K. Copper, A.B. Sproul, A.G. Bruce, A method to calculate array spacing and potential system size of photovoltaic arrays in the urban environment using vector analysis, Appl. Energy. 161 (2016) 11–23. doi:10.1016/j.apenergy.2015.09.074.

[99] NREL, Solar Position Algorithm (SPA), (n.d.). https://midcdmz.nrel.gov/solpos/spa.html (accessed June 19, 2019).

[100] R. Borrmann, K. Rehfeld, A.-K. Wallasch, S. Lüers, Capacity Densities of European Offshore Wind Farms, Varel, 2018.

[101] A. Nghiem, I. Pineda, Wind energy in Europe: Scenarios for 2030, 2017. https://windeurope.org/wp-content/uploads/files/about-wind/reports/Wind-energy-in-Europe-Scenarios-for-2030.pdf%0Ahttp://www.ewea.org/fileadmin/files/library/publications/reports/EWEA-Wind-energy-scenarios-2030.pdf.

[102] European Commission, EU Reference Scenario 2016 - Energy, transport and GHG emissions - Trends to 2050, 2016. doi:10.2833/9127.

[103] G. Bartnes, J.S. Amundsen, I.B. Holm, Kraftmarkedsanalyse 2018 - 2030, 2018. http://publikasjoner.nve.no/rapport/2018/rapport2018_84.pdf.

[104] IEA WIND, 2017 IEA WIND TCP ANNUAL REPORT, 2017.

[105] Economics of Solar Power in Canada, The Economics of Solar Power in Canada, 2019. https://www.neb-one.gc.ca/nrg/sttstc/lctrct/rprt/cnmcsfslrpwr/index-eng.html.

[106] Entsoe, Historical data (until December 2015), (n.d.). https://www.entsoe.eu/data/data-portal/#yearly-values.

[107] Entsoe, Entsog, Annex I, Country Level Results, Scenario report TYDNP 2018, 2018.

[108] D. Vertes, Portfolio Optimization and Efficient Frontiers in R, (2012). http://blog.streeteye.com/blog/2012/01/portfolio-optimization-and-efficient-frontiers-in-r/ (accessed May 15, 2019).

[109] L. Gurobi Optimization, Gurobi Optimizer Reference Manual, (2019).

[110] B. Meindl, M. Templ, Analysis of commercial and free and open source solvers for linear optimization problems, ESSnet Commom Tools Harmon. Methodol. SDC ESS. 1 (2012) 1–14. http://www.statistik.tuwien.ac.at/forschung/CS/CS-2012-1complete.pdf.

[111] L. Söder, P.D. Lund, H. Koduvere, T.F. Bolkesjø, G. Høyvik, E. Rosenlund-soysal, K. Skytte, J. Katz, D. Blumberga, A review of demand side flexibility potential in Northern Europe, Renew. Sustain. Energy Rev. 91 (2018) 654–664. doi:10.1016/j.rser.2018.03.104.

[112] A.-M. Held, Modelling the future development of renewable energy technologies in the European electricity sector using agent-based simulation, (2010).

[113] D.B. Richardson, L.D.D. Harvey, Strategies for correlating solar PV array production with electricity demand, Renew. Energy. 76 (2015) 432–440. doi:10.1016/j.renene.2014.11.053.

[114] D. Heide, L. von Bremen, M. Greiner, C. Hoffmann, M. Speckmann, S. Bofinger, Seasonal optimal mix of wind and solar power in a future, highly renewable Europe, Renew. Energy. 35 (2010) 2483–2489. doi:10.1016/j.renene.2010.03.012.

[115] Flanders Marine Institute, IHO Sea Areas, version 3, (2018). doi:https://doi.org/10.14284/323.

[116] I. Staffell, S. Pfenninger, Using bias-corrected reanalysis to simulate current and future wind power output, Energy. 114 (2016) 1224–1239. doi:10.1016/j.energy.2016.08.068.

[117] J. Olauson, M. Bergkvist, Modelling the Swedish wind power production using MERRA reanalysis data, Renew. Energy. 76 (2015) 717–725. doi:10.1016/j.renene.2014.11.085.

[118] L. Ziegler, E. Gonzalez, T. Rubert, U. Smolka, J.J. Melero, Lifetime extension of onshore wind turbines: A review covering Germany, Spain, Denmark, and the UK, Renew. Sustain. Energy Rev. 82 (2018) 1261–1271. doi:https://doi.org/10.1016/j.rser.2017.09.100.

[119] D.R. Klein, M. Olonscheck, C. Walther, J.P. Kropp, Susceptibility of the European electricity sector to climate change, Energy. 59 (2013) 183–193. doi:10.1016/j.energy.2013.06.048.

[120] F. Ralston Fonseca, P. Jaramillo, M. Bergés, E. Severnini, Seasonal effects of climate change on intra-day electricity demand patterns, Clim. Change. (2019) 435–451.

doi:10.1007/s10584-019-02413-w.

[121] IPCC, Global Warming of 1.5 C, 2018.

Appendix A: Suitability values for CLC classes

Table A-i: CLC classes used for each area based on [16], with the exception of *which are based on [91].

CLC class	Onshore wind	Offshore wind	Solar PV Rooftop	Solar PV farm
111			X	
112			X	
121			X	
211	X			X
212	X			X
221	X			
222	X			
223	X			
231	X			X
241	X			X*
242	X*			
243	X			X
244	X*			
321	X			
311	X*			
312	X*			
313	X*			
322	X			
323	X			
332	X			X
333	X			X

523		X		

Table A-ii: Weight factors for the suitability factor calculation

CLC class	Onshore wind [91]	Offshore wind	Solar PV Rooftop [16]	Solar PV farm[91,97]
111			3	
112			52	
121			11	
211	70			1
212	70			1
221	70			
222	70			
223	70			
231	80			1
241	70			1
242	70			
243	70			1
244	10			
311	10			
312	10			
313	10			
321	80			
322	80			
323	70			
332	80			1
333	80			1
523		100		

Appendix B: Time zones and missing demand data

The first dataset is set at CET [106], while the second one is set at UTC [26]. The data was first adjusted from CET to UTC, this required extrapolation for the first hours for Norway and Denmark. The whole month of January in 2010 of the United Kingdom's hourly demand data was missing, with the exception of the 20th of January 2010. It was assumed that for this period the demand pattern of the UK follows the whole region's demand pattern.

The dataset of the ENTSOE for the period of 2010-2015 "misses" an 1 hour data point each year in October for the region, due to daylight savings. The ERA5 data is set at UCT and therefore does not take into account daylight savings. The missing values were added when daylight savings is reset, between 01:00 and 02:00 in late October. This additional hour was filled in by linear interpolation using the previous and subsequent hour.

Second dataset is set at UCT, there are no missing data points with the exception of the last hour, 23:00 31 December 2018, of Luxembourg which was filled in by linear extrapolation.

Appendix C: Scenario histograms

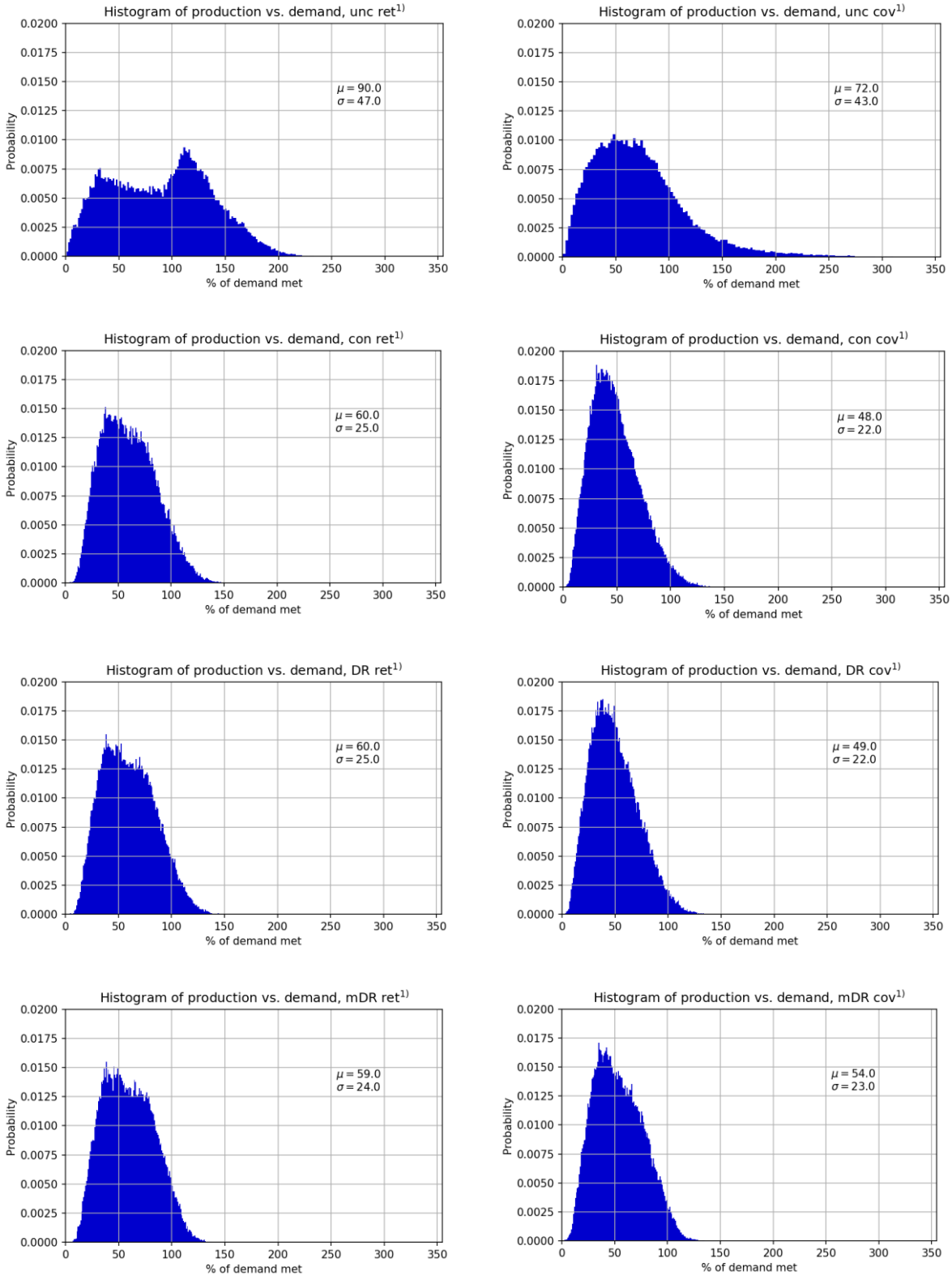

Figure C-i: Histograms of max-return and max-covariance portfolios of four scenarios for 9 years of data. [1)]Unc stands for unconstrained scenario, con for constrained, DR for DR scenario and mDR for maximum correlation DR scenario. ret stands for max-return portfolio, cov for max-covariance portfolio.